

# Flaring of Blazars from an Analytical, Time-dependent Model for Combined Synchrotron and Synchrotron Self-Compton Radiative Losses of Multiple Relativistic Electron Populations

Christian Röken\*

*Universität Regensburg, Fakultät für Mathematik, 93040 Regensburg, Germany*

Florian Schuppan

*Ruhr-Universität Bochum, Institut für Theoretische Physik,  
Lehrstuhl IV: Weltraum- und Astrophysik, 44780 Bochum, Germany*

Katharina Proksch

*Georg-August-Universität Göttingen, Institut für Mathematische Stochastik, 37077 Göttingen, Germany*

Sebastian Schöneberg

*Ruhr-Universität Bochum, Institut für Theoretische Physik,  
Lehrstuhl IV: Weltraum- und Astrophysik, 44780 Bochum, Germany*

(Dated: February 2017)

**ABSTRACT.** A fully analytical, time-dependent leptonic one-zone model that describes a simplified radiation process of multiple interacting relativistic electron populations and accounts for the flaring of blazars is presented. In this model, several mono-energetic, relativistic electron populations are successively and instantaneously injected into the emission region and subjected to linear, time-independent synchrotron and nonlinear, time-dependent synchrotron self-Compton radiative losses. The corresponding electron number density is computed analytically by solving a transport equation using an approximation scheme that employs specific asymptotics. Moreover, the optically thin synchrotron intensity, the synchrotron self-Compton intensity in the Thomson limit, as well as the associated total fluences are explicitly calculated. In order to mimic injections of finite duration times and radiative transport, flares are modeled by sequences of these instantaneous injections, suitably distributed over the entire emission region. The total synchrotron and synchrotron self-Compton fluence spectral energy distributions are plotted for a generic three-flare scenario with a set of realistic parameter values, reproducing the typical broad-band behavior seen in observational data.

## Contents

<b>I. Introduction</b>	2
<b>II. The Relativistic Transport Equation</b>	3
A. Formal Solution of the Relativistic Transport Equation	4
B. Solution of the Relativistic Transport Equation for $\{t \in \mathbb{R}_{\geq 0} \mid t_j \leq t < t_{j+1} \text{ with } j \in \{1, \dots, m\}\}$	5
1. NID Solution	6
2. FID Solution	8
C. Solution of the Relativistic Transport Equation for $\{t \in \mathbb{R}_{\geq 0}\}$	9
<b>III. Synchrotron and SSC Intensities</b>	12
A. Synchrotron Intensity	12
B. SSC Intensity	13
<b>IV. Synchrotron and SSC Fluences</b>	14
A. Synchrotron Fluence	15
B. SSC Fluence	16
<b>V. Lightcurves and Fluence SEDs</b>	17

---

\* e-mail: christian.roeken@mathematik.uni-regensburg.de

<b>VI. Summary and Outlook</b>	18
<b>Acknowledgments</b>	19
<b>A. Laplace Method</b>	19
<b>B. NID-FID Transition Time</b>	20
<b>C. Constants of Integration – Initial and Transition Conditions and Updating</b>	21
<b>D. Components of <math>G(t 0 \leq t &lt; \infty)</math> and Initial Values <math>G_i</math></b>	22
<b>E. The <math>CS</math> Function</b>	23
<b>F. Lorentz Transformations</b>	24
<b>G. Numerical Code for Fluence SEDs</b>	24
<b>References</b>	25

## I. INTRODUCTION

Blazars are among the most energetic phenomena in nature, representing the most extreme type in the class of active galactic nuclei [37]. Their main jet outflow in form of magnetized plasmoids, which are assumed to arise in the Blandford-Znajek and the Blandford-Payne process [6, 7], constitutes the major radiation zones. These plasmoids pick up – and interact with – particles of interstellar and intergalactic clouds along their trajectories [27], giving rise to the emission of a series of strong flares.

A blazar spectral energy distribution (SED) consists of two broad non-thermal radiation components in different domains. The low-energy spectral component, ranging from radio to optical or X-ray energies, is usually attributed to synchrotron radiation of relativistic electrons subjected to ambient magnetic fields. The origin of the high-energy spectral component, covering the X-ray to  $\gamma$ -ray regime, is still under debate. It can be modeled by inverse Compton radiation coming from low-energy photon fields that interact with the relativistic electrons [10]. This process can be described either by a synchrotron self-Compton (SSC) model, where the electrons scatter their self-generated synchrotron photons, or by so-called external Compton models, where the seed photons are generated in the accretion disk [17], the broad-line region [35], or the dust torus [8] of the central black hole. Instead of such a leptonic scenario, the high-energy component can also be modeled by hadronic scenarios via proton-synchrotron radiation or the emission of  $\gamma$ -rays from the decay of neutral pions formed in interactions of protons with ambient matter (see, e.g., [12, 14, 38] and references therein). Mixed models including both leptonic as well as hadronic processes are also considered in the literature (e.g., [13, 39]).

A main feature of the non-thermal blazar emission is a distinct variability at all frequencies with different time scales ranging from years down to a few minutes. The shortest variability time scales are usually observed for the highest energies of the spectral components, as in PKS 2155-304 [2, 3] and Mrk 501 [4] in the TeV range, or Mrk 421 [16] in the X-ray domain. So far, only multi-zone models, which feature an internal structure of the emission region with various radiation zones caused by collisions of moving and stationary shock waves, have been proposed to explain the extreme short-time variability of blazars (see, e.g., [5, 20–22, 26, 36]). In the framework of one-zone models, however, extreme short-time variability can, a priori, not be realized as the duration of the injection into an emission knot of finite size with characteristic radius  $\mathcal{R}_0$  and the light crossing (escape) time in this region are naturally of the order  $\mathcal{O}(2\mathcal{R}_0/(cD))$ ,  $c$  being the speed of light in vacuum and  $D$  the Doppler factor [18]. This leads to a minimum time scale for the observed flare duration, which may exceed the short-time variability scale in the minute range by several magnitudes. In particular, using the typical parameters  $\mathcal{R}_0 = 10^{15}$  cm and  $D = 10$ , we find  $2\mathcal{R}_0/(cD) \approx 1.9$  h in the observer frame. Thus, this type of model can only be used to account for variability on larger time scales, that is, from years down to hours.

Both one-zone and multi-zone models have been studied extensively over the last decades in order to explain the variability and the SEDs of blazars, incorporating leptonic and hadronic interactions. In these studies, analytical as well as numerical approaches were used, containing, among others, various radiative loss and acceleration processes, details of radiative transport, diverse injection patterns, different cross sections for particle interactions, as well as particle decay and pair production/annihilation (see the review article [11] and the references therein). Thus, the literature on this matter is quite comprehensive. However, models featuring pick-up processes of any kind usually assume only a single injection of particles into the emission knot as the cause of the flaring.

This may be unrealistic as blazar jets, which can extend over tens of kiloparsecs, most likely intersect with several clouds, leading to multiple injections. In such an intricate situation, it is of particular interest to have a self-consistent description of the particle's radiative cooling, the radiative transport, et cetera. Therefore, we propose a simple, but fully analytical, time-dependent leptonic one-zone model featuring multiple uniform injections of nonlinearly interacting relativistic electron populations, which undergo combined synchrotron and SSC radiative losses (for previous works, see [29, 30]). More precisely, we assume that the blazar radiation emission originates in spherically shaped and fully ionized plasmoids, which feature intrinsic randomly-oriented, but constant, large-scale magnetic fields and propagate relativistically along the general direction of the jet axis. These plasmoids pass through – and interact with – clouds of the interstellar and intergalactic media, successively and instantaneously picking up multiple mono-energetic, spatially isotropically distributed electron populations, which are subjected to linear, time-independent synchrotron radiative losses via interactions with the ambient magnetic fields and to nonlinear, time-dependent SSC radiative losses in the Thomson limit. This is the first time an analytical model that describes combined synchrotron and SSC radiative losses of several subsequently injected, interacting injections is presented (for a minor, purely numerical study on multiple injections see [25]). We point out that because the SSC cooling is a collective effect, that is, the cooling of a single electron depends on the entire ensemble within the emission region, injections of further particle populations into an already cooling system give rise to alterations of the overall cooling behavior [30, 40]. Moreover, as we do employ Dirac distributions for the time profile of the source function of our evolution equation and, further, do not consider any details of radiative transport, we mimic injections of finite duration times and radiative transport by partitioning each flare into a sequence of instantaneous injections, which are appropriately distributed over the entire emission region, using the quantities computed here.

The article is organized as follows. In Section II, an approximate analytical solution of the time-dependent, relativistic transport equation of the volume-averaged differential electron number density is derived. Based on this solution, the optically thin synchrotron intensity, the SSC intensity in the Thomson limit, as well as the corresponding total fluences are calculated in Sections III and IV. We explain how to mimic finite injection durations and radiative transport by multiple use of our results in Section V, and show that the model accounts for the characteristic broad-band fluence SED behavior of blazars obtained from observational data. Section VI concludes with a summary and an outlook. Supplementary material, which is required for the computations of the electron number density and the synchrotron and SSC intensities, is given in Appendices A-F. Moreover, in Appendix G, we briefly describe the numerical code used for the creation of the fluence SED plot.

## II. THE RELATIVISTIC TRANSPORT EQUATION

The transport equation describing the temporal evolution and energy dependence of the volume-averaged differential electron number density  $n = n(\gamma, t)$  of  $m$  relativistic, mono-energetic, instantaneously injected and spatially isotropically distributed electron populations in the rest frame of a non-thermal radiation source with dominant magnetic field self-generation and radiative losses  $L = L(\gamma, t)$  reads [24]

$$\frac{\partial n}{\partial t} - \frac{\partial}{\partial \gamma}(L n) = \sum_{i=1}^m q_i \delta(\gamma - \gamma_i) \delta(t - t_i), \quad (1)$$

where  $\delta(\cdot)$  is the Dirac distribution,  $q_i$  the  $i$ th injection strength,  $\gamma_i := E_{e,i}/(m_e c^2) \gg 1$  the  $i$ th normalized initial electron energy, and  $t_i$  the  $i$ th injection time for  $i : 1 \leq i \leq m$ . In this work, radiative losses in form of both a linear, time-independent synchrotron cooling process (with a constant magnetic field  $\mathbf{B}$ ) and a nonlinear, time-dependent SSC cooling process in the Thomson limit are considered

$$L = L_{\text{syn.}} + L_{\text{SSC}} = \gamma^2 \left( D_0 + A_0 \int_0^\infty \gamma^2 n \, d\gamma \right). \quad (2)$$

The quantities  $D_0 = 1.3 \times 10^{-9} b^2 \text{ s}^{-1}$  and  $A_0 = 1.2 \times 10^{-18} b^2 \text{ cm}^3 \text{ s}^{-1}$  are the respective cooling magnitudes depending on the magnetic field strength  $b := \|\mathbf{B}\|/\text{Gauss} = \text{const.}$ , which is normalized to one Gauss [9, 32]. In the present context, the term *linear* means that the synchrotron losses do not depend on the electron number density  $n$ , thus, resulting in a linear term in the partial differential equation (PDE) (1), whereas the SSC loss term depends on an energy integral containing  $n$ , yielding a nonlinearity. The synchrotron loss term can, in principle, be modeled as nonlinear and time-dependent, too. This can be achieved by making an equipartition assumption between the magnetic and particle energy densities [33]. Note that, except for TeV blazars, where Klein-Nishina effects drastically reduce the SSC cooling strength above a certain energy threshold, the dominant contribution of the SSC energy loss rate originates in the Thomson regime [32]. Therefore, restricting this model to GeV blazars, it is sufficient for the evolution of the electron number density to employ SSC radiative losses in

the Thomson limit. As a consequence, the normalized initial electron energies have to be bounded from above by  $\gamma_i < 1.9 \times 10^4 b^{-1/3}$ . We also point out that the only accessible energy in synchrotron and SSC cooling processes is the kinetic energy of the electrons. Thus,  $\gamma$  denotes the kinetic component of the normalized total energy  $E_{\text{tot.}}/(m_e c^2)$ , i.e.,

$$\gamma = \frac{E_{\text{tot.}} - m_e c^2}{m_e c^2} = \gamma_{\text{tot.}} - 1.$$

Hence,  $\gamma_{\text{tot.}} \in [1, \infty)$  implies  $\gamma \in [0, \infty)$ . For this reason, the lower integration bound in (2) is zero. Furthermore, the Dirac distributions  $\delta(\gamma - \gamma_i)$  and  $\delta(t - t_i)$  in Eq.(1) describe a sequence of energy and time points  $(\gamma_i, t_i)_{i \in \{1, \dots, m\}}$ . They are to be understood in the distributional sense, that is, they are linear functionals on the space of (smooth) test functions  $\varphi$  on  $\mathbb{R}$  with compact support

$$C_0^\infty(\mathbb{R}) := \{\varphi \mid \varphi \in C^\infty(\mathbb{R}), \text{ supp } \varphi \text{ compact}\}.$$

More precisely, for  $k \in \mathbb{R}$ , one can rigorously define them as the mapping

$$\delta : C_0^\infty(\mathbb{R}) \rightarrow \mathbb{R}, \quad \varphi \mapsto \varphi(0)$$

with the integral of the Dirac distribution against a test function given by

$$\int_{-\infty}^{\infty} \varphi(k) \delta(k) dk = \varphi(0) \quad \text{for all } \varphi \in C_0^\infty(\mathbb{R}).$$

#### A. Formal Solution of the Relativistic Transport Equation

In terms of the function  $R(\gamma, t) := \gamma^2 n(\gamma, t)$  and the variable  $x := 1/\gamma$ , we can rewrite Eq.(1) in the form

$$\frac{\partial R}{\partial t} + J \frac{\partial R}{\partial x} = \sum_{i=1}^m q_i \delta(x - x_i) \delta(t - t_i), \quad (3)$$

where

$$J = J(t) := D_0 + A_0 \int_0^\infty \frac{R(x, t)}{x^2} dx. \quad (4)$$

Defining the strictly increasing, continuous function  $G = G(t)$  via

$$0 < \frac{dG}{dt} := J, \quad (5)$$

Eq.(3) becomes

$$\frac{\partial R}{\partial G} + \frac{\partial R}{\partial x} = \sum_{i=1}^m q_i \delta(x - x_i) \delta(G - G_i) \quad (6)$$

with  $G_i := G(t_i)$ . Albeit the nonlinear transport equation (1) is now transformed into a linear PDE, its solution can obviously serve as a Green's function only for the single injection scenario with  $m = 1$ . Consequently, in order to solve the generalized transport equation

$$\frac{\partial n}{\partial t} - \frac{\partial}{\partial \gamma}(L n) = Q$$

for  $m > 1$ , where  $Q = Q(\gamma, t)$  is a more suitable source function, one cannot simply use Green's method. Applying successive Laplace transformations with respect to  $x$  and  $G$  to Eq.(6) yields the solution

$$R(x, G) = \sum_{i=1}^m q_i H(G - G_i) \delta(x - x_i - G + G_i), \quad (7)$$

where  $H(\cdot)$  is the Heaviside step function

$$H(k - k_0) := \begin{cases} 0 & \text{for } k < k_0 \\ 1 & \text{for } k > k_0 \end{cases}$$

with  $k, k_0 \in \mathbb{R}$ , which has a jump discontinuity at  $k = k_0$ . A detailed derivation of this solution can be found in Appendix A. In order to determine the function  $G$ , we substitute solution (7) into (4) and, by using (5), obtain the ordinary differential equation (ODE)

$$\frac{dG}{dt} = D_0 + A_0 \sum_{i=1}^m \frac{q_i H(G - G_i)}{(G - G_i + x_i)^2}. \quad (8)$$

This equation can be regarded as a compact notation for the set of  $m$  piecewise-defined ODEs

$$\left\{ \begin{array}{ll} \frac{dG}{dt} = D_0 + A_0 \frac{q_1}{(G - G_1 + x_1)^2} & \text{for } G_1 \leq G < G_2 \\ \frac{dG}{dt} = D_0 + A_0 \left( \frac{q_1}{(G - G_1 + x_1)^2} + \frac{q_2}{(G - G_2 + x_2)^2} \right) & \text{for } G_2 \leq G < G_3 \\ \vdots & \vdots \\ \frac{dG}{dt} = D_0 + A_0 \left( \frac{q_1}{(G - G_1 + x_1)^2} + \frac{q_2}{(G - G_2 + x_2)^2} + \dots + \frac{q_m}{(G - G_m + x_m)^2} \right) & \text{for } G_m \leq G < \infty. \end{array} \right. \quad (9)$$

In Section II B, an approximate analytical solution for the general case of  $j$  injections, i.e., for the interval  $G_j \leq G < G_{j+1}$ , where  $j \in \{1, \dots, m\}$  and  $G_1 = 0$ ,  $G_{m+1} = \infty$ , is presented. Having a separate analytical solution for each ODE of (9), in Section II C, these are glued together successively requiring continuity at the transition points. Finally, with (7), the electron number density results in

$$\begin{aligned} n(\gamma, t) &= \gamma^{-2} R(\gamma, t) = \gamma^{-2} \sum_{i=1}^m q_i H(G(t) - G_i) \delta\left(\frac{1}{\gamma} - \frac{1}{\gamma_i} - G(t) + G_i\right) \\ &= \sum_{i=1}^m q_i H(t - t_i) \delta\left(\gamma - \frac{\gamma_i}{1 + \gamma_i (G(t) - G_i)}\right). \end{aligned} \quad (10)$$

### B. Solution of the Relativistic Transport Equation for $\{t \in \mathbb{R}_{\geq 0} \mid t_j \leq t < t_{j+1} \text{ with } j \in \{1, \dots, m\}\}$

In the interval  $G_j \leq G < G_{j+1}$ , Eq.(8) gives

$$\frac{dG}{dt} = D_0 + A_0 \sum_{i=1}^j \frac{q_i}{(G - G_i + x_i)^2}. \quad (11)$$

We now introduce the time-dependent sets  $S_1$  and  $S_2$  that contain injections with  $G - G_i \ll x_i$  and  $G - G_i \gg x_i$  for  $i : 1 \leq i \leq j$ , respectively. In order to rewrite Eq.(11) in terms of these sets, we continue their domains of validity to  $G - G_i < x_i$  and  $G - G_i \geq x_i$ . However, for the computations below, we still use the former *much less than* and *much greater than* relations when we carry out approximations. Then, Eq.(11) can be represented formally by

$$\frac{dG}{dt} = D_0 + A_0 \sum_{k \in S_1} \frac{q_k}{(G - G_k + x_k)^2} + A_0 \sum_{l \in S_2} \frac{q_l}{(G - G_l + x_l)^2}. \quad (12)$$

With the generalized geometric series

$$\frac{1}{(1 - z)^2} = \sum_{n=0}^{\infty} (n+1) z^n, \quad |z| < 1,$$

we can express Eq.(12) as

$$\begin{aligned} \frac{dG}{dt} &= D_0 + A_0 \sum_{k \in S_1} \frac{q_k}{x_k^2} \left(1 + \frac{G - G_k}{x_k}\right)^{-2} + \frac{A_0}{G^2} \sum_{l \in S_2} q_l \left(1 - \frac{G_l - x_l}{G}\right)^{-2} \\ &= D_0 + A_0 \sum_{k \in S_1} \sum_{n=0}^{\infty} \frac{(n+1)q_k}{x_k^2} \left(-\frac{G - G_k}{x_k}\right)^n + \frac{A_0}{G^2} \sum_{l \in S_2} \sum_{p=0}^{\infty} (p+1)q_l \left(\frac{G_l - x_l}{G}\right)^p. \end{aligned}$$

This ODE is suitably approximated by considering only the leading- and next-to-leading-order terms

$$\begin{aligned} \frac{dG}{dt} &\approx D_0 + A_0 \sum_{k \in S_1} \frac{q_k}{x_k^2} \left(1 - 2 \frac{G - G_k}{x_k}\right) + \frac{A_0}{G^2} \sum_{l \in S_2} q_l \left(1 + 2 \frac{G_l - x_l}{G}\right) \\ &= M_1(j, S_1) + M_2(j, S_1) G + \frac{N_1(j, S_2)}{G^2} + \frac{N_2(j, S_2)}{G^3}, \end{aligned} \tag{13}$$

where the “constants”

$$M_1(j, S_1) := D_0 + A_0 \sum_{k \in S_1} \frac{q_k}{x_k^2} \left(1 + \frac{2G_k}{x_k}\right), \quad M_2(j, S_1) := -2 A_0 \sum_{k \in S_1} \frac{q_k}{x_k^3},$$

$$N_1(j, S_2) := A_0 \sum_{l \in S_2} q_l, \quad \text{and} \quad N_2(j, S_2) := 2 A_0 \sum_{l \in S_2} q_l (G_l - x_l)$$

depend on the numbers of elements of  $S_1$  and  $S_2$ , which may change over time. Note that the explicit dependences of these constants on the actual number of injections as well as numbers of elements of  $S_1$  and  $S_2$  are suppressed in the subsequent calculations for simplicity if possible and given if necessary. An approximate analytical solution of Eq.(13) can be obtained by first computing asymptotic – and then continued – solutions for the near-injection domain (NID)  $G_j \leq G < \min(G_{j+1}, G_T(j))$  and for the far-injection domain (FID)  $\min(G_{j+1}, G_T(j)) \leq G < G_{j+1}$ , which, in case  $G_T(j) < G_{j+1}$ , are glued together continuously at the transition point  $G_T = G_T(j) := G_j + x_j$  that defines the transition between  $S_1$  and  $S_2$  for the  $j$ th injection and corresponds to the transition time  $t_T = t_T(j)$  specified in Appendix B. For  $G_{j+1} \leq G_T(j)$ , we regard solely the NID solution. In the following, the general strategy is to use the leading- and next-to-leading-order contributions in Eq.(13) only if a single set  $S_1$  or  $S_2$  has to be taken into account, whereas only the leading-order terms are considered if both sets have to be employed.

### 1. NID Solution

In the NID  $G_j \leq G < \min(G_{j+1}, G_T(j))$ , at least the  $j$ th injection is an element of  $S_1$ . Further, one may – but does not necessarily need to – have injections in  $S_2$ . Therefore, we distinguish the two cases  $S_2 = \emptyset$  and  $S_2 \neq \emptyset$ . First, if  $S_2 = \emptyset$ , Eq.(13) yields

$$\frac{dG}{dt} = M_1(j) + M_2(j) G \quad \text{for} \quad G_j \leq G < \min(G_{j+1}, G_T(j)). \tag{14}$$

This ODE can be solved easily using separation of variables. We obtain

$$\int \frac{dG}{M_1 + M_2 G} = \frac{1}{M_2} \ln(M_1 + M_2 G) = t + c_1, \quad c_1 = \text{const.} \in \mathbb{R},$$

which is equivalent to

$$G(t) = \frac{M_1}{|M_2|} - c_2 \exp(-|M_2| t)$$

with  $c_2 := \exp(-|M_2| c_1) / |M_2| \in \mathbb{R}_{>0}$ . The constant  $c_2$  is fixed by applying the initial condition  $G(t = t_j) = G_j$ , giving

$$c_2 = \left( \frac{M_1}{|M_2|} - G_j \right) \exp(|M_2| t_j)$$

and, hence,

$$G(t) = \frac{M_1(j)}{|M_2(j)|} - \left( \frac{M_1(j)}{|M_2(j)|} - G_j \right) \exp(-|M_2(j)|(t - t_j)) \quad \text{for } t_j \leq t < \min(t_{j+1}, t_T(j)). \quad (15)$$

In the case  $S_2 \neq \emptyset$ , by considering the leading-order terms only, Eq.(13) results in

$$\frac{dG}{dt} = P_1 + \frac{N_1}{G^2} \quad \text{for } G_j \leq G < \min(G_{j+1}, G_T(j)), \quad (16)$$

where  $P_1 = P_1(j, S_1) := D_0 + A_0 \sum_{k \in S_1} q_k/x_k^2$ . Again employing separation of variables and extending the integrand with the multiplicative identity  $P_1/P_1$  and the neutral element  $N_1 - N_1$ , we find

$$\int \frac{G^2 dG}{N_1 + P_1 G^2} = \frac{1}{P_1} \left( G - N_1 \int \frac{dG}{N_1 + P_1 G^2} \right) = \frac{1}{P_1} \left( G - \sqrt{\frac{N_1}{P_1}} \arctan \left( \sqrt{\frac{P_1}{N_1}} G \right) \right) = t + c_3 \quad (17)$$

with  $c_3 = \text{const.} \in \mathbb{R}$ . One way of deriving an approximate analytical solution of this transcendental equation is to determine  $G$  asymptotically for small and large arguments of the arctan function (in case both asymptotic ends exist for  $G : G_j \leq G < \min(G_{j+1}, G_T)$ ), extrapolate these solutions up to an intermediate transition point such that the entire domain of definition is covered, and apply a branch-gluing at the transition point requiring continuity. For small arguments  $\sqrt{P_1/N_1} G \ll 1$ , we use the third-order approximation  $\arctan(x)|_{x \ll 1} \approx x - x^3/3$ , as the linear term in Eq.(17) and the linear contribution in the approximation of the arctan function cancel each other. This leads to the asymptotic solution

$$G(t) \simeq (3 N_1 t + c)^{1/3}, \quad c = \text{const.} \in \mathbb{R}. \quad (18)$$

For large arguments  $\sqrt{P_1/N_1} G \gg 1$ , the arctan function can be well approximated by  $\pi/2$ . We directly obtain an asymptotic solution of the form

$$G(t) \simeq P_1 t + c', \quad c' = \text{const.} \in \mathbb{R}. \quad (19)$$

By means of the condition  $\sqrt{P_1/N_1} G = 1$ , we derive the NID transition value

$$G_T^{(n)} = \sqrt{\frac{N_1}{P_1}}. \quad (20)$$

This value specifies the upper bound of the domain of validity of (18) and the lower bound of the domain of validity of (19). The corresponding transition time can be directly computed by substituting (20) into (17), in which the constant  $c_3$  had to be fixed via the initial condition  $G(t = t_j) = G_j$  resulting in

$$c_3 = \frac{1}{P_1} \left( G_j - \sqrt{\frac{N_1}{P_1}} \arctan \left( \sqrt{\frac{P_1}{N_1}} G_j \right) \right) - t_j.$$

This yields

$$t_T^{(n)} = t_j + \frac{1}{P_1} \left( \sqrt{\frac{N_1}{P_1}} \left[ 1 - \frac{\pi}{4} + \arctan \left( \sqrt{\frac{P_1}{N_1}} G_j \right) \right] - G_j \right). \quad (21)$$

We point out that in general, one does not have the ordered sequence  $G_j < G_T^{(n)} < G_T$  because  $G_T^{(n)}$  can in principle be larger than or equal to  $G_T$  as well as smaller than or equal to  $G_j$ . These cases arise when only one asymptotic end of the arctan function exists. Hence, for  $G_j < G_T^{(n)}(j) < G_T(j)$ , the solution of Eq.(17) is approximately given by

$$G(t) = \begin{cases} (3 N_1(j) t + c_4(j))^{1/3} & \text{for } t_j \leq t < \min(t_{j+1}, t_T^{(n)}(j)) \\ P_1(j) t + c_5(j) & \text{for } \min(t_{j+1}, t_T^{(n)}(j)) \leq t < \min(t_{j+1}, t_T(j)), \end{cases} \quad c_4, c_5 = \text{const.} \in \mathbb{R}, \quad (22)$$

for  $G_j < G_T(j) \leq G_T^{(n)}(j)$  by

$$G(t) = (3 N_1(j) t + c_6(j))^{1/3} \quad \text{for } t_j \leq t < \min(t_{j+1}, t_T(j)), \quad c_6 = \text{const.} \in \mathbb{R}, \quad (23)$$

and for  $G_T^{(n)}(j) \leq G_j$  by

$$G(t) = P_1(j)t + c_7(j) \quad \text{for } t_j \leq t < \min(t_{j+1}, t_T(j)), \quad c_7 = \text{const.} \in \mathbb{R}. \quad (24)$$

The integration constants  $c_4, \dots, c_7$  are determined in Appendix C. In order to compute the constants  $M_1, M_2, N_1$ , and  $P_1$ , we have to continually check during the evolution of  $G \in [G_j, \min(G_{j+1}, G_T(j))]$  whether an injection belongs to the set  $S_1$  or the set  $S_2$ . Therefore, we specify two different kinds of updates. The first kind occurs when a new injection enters the system, while the second kind is due to NID-FID transitions. We start with the initial update at the time of the  $j$ th injection verifying

$$\begin{aligned} G_j - G_i &< x_i & \text{for the } i\text{th injection being in } S_1 \\ G_j - G_i &\geq x_i & \text{for the } i\text{th injection being in } S_2, \end{aligned}$$

where  $i \in \{1, \dots, j\}$ . Next, since all transition values  $G_T(i)$  are known, they can be arranged as an ordered  $j$ -tuple representing an increasing time sequence. Assuming that a certain number of  $G_T(i)$ -values is contained in the time interval under consideration, whenever  $G$  reaches one of them, both sets  $S_1$  and  $S_2$  have to be updated accordingly, i.e., the corresponding injection is removed from  $S_1$ , while at the same time it is added to  $S_2$ . For more details on the updating see Section II C and Appendix C.

## 2. FID Solution

In the FID  $\min(G_{j+1}, G_T(j)) \leq G < G_{j+1}$ , the  $j$ th injection is, per definition, an element of  $S_2$ . Moreover,  $S_1$  can only contain injections with comparatively low initial electron energies. However, in the present setting, such injections practically do not occur because the initial electron energies defined in the rest frame of the plasmoid, which primarily result from the relativistic motion of the plasmoid with respect to the ambient medium, are typically of the same order. Consequently, taking into account the leading- and next-to-leading-order terms with respect to  $S_2$ , Eq.(13) becomes

$$\frac{dG}{dt} = D_0 + \frac{N_1(j)}{G^2} + \frac{N_2(j)}{G^3} \quad \text{for } G_T(j) \leq G < G_{j+1}. \quad (25)$$

An approximate analytical solution of this ODE can be obtained in a similar way as the NID solution by first applying separation of variables, resulting in an integral equation of the form

$$\int \frac{G^3 dG}{D_0 G^3 + N_1 G + N_2} = t + d_1, \quad d_1 = \text{const.} \in \mathbb{R}. \quad (26)$$

This integral equation is shown to be approximately equivalent to a specific transcendental equation for which we subsequently derive asymptotic solutions for  $G$  that are continued up to an intermediate transition point (if both asymptotic ends exist, else we only consider a continuation of the solution of the present asymptotic end over the entire domain), where they are glued together continuously. In more detail, since  $N_1 G \gg N_2$ , we employ a first-order geometric series approximation in  $N_2/(N_1 G)$  in the integrand of (26)

$$\begin{aligned} \int \frac{G^3 dG}{D_0 G^3 + N_1 G + N_2} &= \frac{G}{D_0} - \frac{1}{D_0} \int \frac{N_1 G + N_2}{D_0 G^3 + N_1 G + N_2} dG = \frac{G}{D_0} - \frac{1}{D_0} \int \frac{dG}{1 + \frac{D_0 G^3}{N_1 G + N_2}} \\ &= \frac{G}{D_0} - \frac{1}{D_0} \int \frac{dG}{1 + \frac{D_0 G^2}{N_1} \left(1 + \frac{N_2}{N_1 G}\right)^{-1}} = \frac{G}{D_0} - \frac{1}{D_0} \int \frac{dG}{1 + \frac{D_0 G^2}{N_1} \sum_{n=0}^{\infty} \left(-\frac{N_2}{N_1 G}\right)^n} \\ &\approx \frac{G}{D_0} - \frac{1}{D_0} \int \frac{dG}{1 + \frac{D_0}{N_1} \left(G - \frac{N_2}{2N_1}\right)^2 - \frac{D_0 N_2^2}{4N_1^3}} \approx \frac{G}{D_0} - \frac{1}{D_0} \int \frac{dG}{1 + \frac{D_0}{N_1} \left(G - \frac{N_2}{2N_1}\right)^2}. \end{aligned} \quad (27)$$

Note that in the first step, we included the multiplicative identity  $D_0/D_0$  and the neutral element  $(N_1 G + N_2) - (N_1 G + N_2)$  in the numerator of the integrand, giving the splitting into two terms. Then, by means of simple



algebraic manipulations, we expressed the integrand in a form suitable for the substitution of the geometric series. For reasons of computational simplicity, we dropped the small second-order contribution  $-D_0 N_2^2/(4 N_1^3)$  in the last step. The final integral in (27) is solved by an arctan function. Thus, introducing the parameter  $\beta = \beta(j) := D_0^{1/2} N_2(j)/(2 N_1^{3/2}(j))$ , Eq.(26) results in

$$\frac{G}{D_0} - \frac{N_1^{1/2}}{D_0^{3/2}} \arctan \left( \beta \left[ \frac{2 N_1 G}{N_2} - 1 \right] \right) = t + d_1. \quad (28)$$

In order to find an approximate analytical solution of this transcendental equation, we determine  $G$  asymptotically for both small and large arguments of the arctan function. Therefore, using the third-order approximation of the arctan function for small arguments  $\beta (2 N_1 G/N_2 - 1) \ll 1$ , the associated asymptotic solution becomes

$$G(t) \simeq (3 N_1 t + d)^{1/3} + \frac{N_2}{2 N_1}, \quad d = \text{const.} \in \mathbb{R}.$$

Also, because  $\arctan(x)|_{x \gg 1} \approx \pi/2$ , the asymptotic solution for large arguments  $\beta (2 N_1 G/N_2 - 1) \gg 1$  reads

$$G(t) \simeq D_0 t + d', \quad d' = \text{const.} \in \mathbb{R}.$$

Extending the domains of these solutions up to – and connecting them continuously at – the transition point

$$G_T^{(f)} = \sqrt{\frac{N_1}{D_0}} + \frac{N_2}{2 N_1}, \quad (29)$$

which is derived from the transition condition  $\beta (2 N_1 G/N_2 - 1) = 1$  and corresponds to the transition time

$$t_T^{(f)} = t_T + \frac{1}{D_0} \left( -G_j - x_j + \frac{N_2}{2 N_1} + \sqrt{\frac{N_1}{D_0}} \left[ 1 - \frac{\pi}{4} + \arctan \left( \beta \left[ \frac{2 N_1 (G_j + x_j)}{N_2} - 1 \right] \right) \right] \right), \quad (30)$$

we obtain for  $G_T(j) < G_T^{(f)}(j) < G_{j+1}$  the piecewise-defined solution

$$G(t) = \begin{cases} (3 N_1(j) t + d_2(j))^{1/3} + \frac{N_2(j)}{2 N_1(j)} & \text{for } t_T(j) \leq t < t_T^{(f)}(j) \\ D_0 t + d_3(j) & \text{for } t_T^{(f)}(j) \leq t < t_{j+1}, \quad d_2, d_3 = \text{const.} \in \mathbb{R}. \end{cases} \quad (31)$$

In case only one asymptotic end exists, that is for  $G_T(j) < G_{j+1} \leq G_T^{(f)}(j)$  and  $G_T^{(f)}(j) \leq G_T(j)$ , we get

$$G(t) = (3 N_1(j) t + d_4)^{1/3} + \frac{N_2(j)}{2 N_1(j)} \quad \text{for } t_T(j) \leq t < t_{j+1}, \quad d_4 = \text{const.} \in \mathbb{R}, \quad (32)$$

and

$$G(t) = D_0 t + d_5(j) \quad \text{for } t_T(j) \leq t < t_{j+1}, \quad d_5 = \text{const.} \in \mathbb{R}, \quad (33)$$

respectively. We remark that similar to the calculation of the transition time (21) of the NID, the transition time (30) was computed fixing the integration constant

$$d_1 = -t_T + \frac{1}{D_0} \left( G_j + x_j - \sqrt{\frac{N_1}{D_0}} \arctan \left( \beta \left[ \frac{2 N_1 (G_j + x_j)}{N_2} - 1 \right] \right) \right)$$

in Eq.(28) by imposing the boundary condition  $G(t = t_T) = G_T$ , and substituting the transition value (29). The determination of the integration constants  $d_2, \dots, d_5$  is given in Appendix C. Further, the constants  $N_1$  and  $N_2$  are specified by identifying which injections are initially (that is now at  $t = t_T$ ) in  $S_2$ , verifying the condition  $G_T(j) - G_i \geq x_i$  for all  $i \in \{1, \dots, j\}$ .

### C. Solution of the Relativistic Transport Equation for $\{t \in \mathbb{R}_{\geq 0}\}$

The complete solution of Eq.(8) is derived as follows. Beginning with the single-injection domain (SID), the solution branch  $G(t | 0 \leq t < t_2)$  is given for  $0 \leq t < \min(t_2, t_T(1))$  by Sol.(15) and for  $t_T(1) \leq t < t_2$  by

- Sol.(31) for  $t_T(1) < t_T^{(f)}(1) < t_2$ ,
- Sol.(32) for  $t_T(1) < t_2 \leq t_T^{(f)}(1)$ ,
- Sol.(33) for  $t_T^{(f)}(1) \leq t_T(1)$

with  $j = 1$ . We point out that in this domain, Eq.(8) can also be solved by directly applying separation of variables, resulting in [34]

$$\int \frac{\mathcal{G}^2}{D_0 \mathcal{G}^2 + A_0 q_1} d\mathcal{G} = \frac{\mathcal{G}}{D_0} - \frac{1}{D_0} \int \frac{d\mathcal{G}}{1 + \frac{D_0 \mathcal{G}^2}{A_0 q_1}} = \frac{\mathcal{G}}{D_0} - \frac{(A_0 q_1)^{1/2}}{D_0^{3/2}} \arctan \left( \sqrt{\frac{D_0}{A_0 q_1}} \mathcal{G} \right) = t + e_1, \quad (34)$$

where  $\mathcal{G} := G + x_1$  and  $e_1 = \text{const.} \in \mathbb{R}$ . Using the asymptotic-branch-gluing method (cf. Sections IIB 1 and IIB 2) with the transition time

$$t_T^{(s)} = \frac{1}{D_0} \left[ -x_1 + \sqrt{\frac{A_0 q_1}{D_0}} \left( 1 - \frac{\pi}{4} + \arctan \left[ \sqrt{\frac{D_0}{A_0 q_1}} x_1 \right] \right) \right]$$

leads for  $0 < t_T^{(s)} < t_2$  to the approximate solution

$$G(t) = \begin{cases} (3 A_0 q_1 t + e_2)^{1/3} - x_1 & \text{for } 0 \leq t < t_T^{(s)} \\ D_0 t + e_3 & \text{for } t_T^{(s)} \leq t < t_2, \end{cases} \quad e_2, e_3 = \text{const.} \in \mathbb{R}, \quad (35)$$

for  $0 < t_2 \leq t_T^{(s)}$  to

$$G(t) = (3 A_0 q_1 t + e_4)^{1/3} - x_1 \quad \text{for } 0 \leq t < t_2, \quad e_4 = \text{const.} \in \mathbb{R}, \quad (36)$$

and otherwise for  $t_T^{(s)} \leq 0$  to

$$G(t) = D_0 t + e_5 \quad \text{for } 0 \leq t < t_2, \quad e_5 = \text{const.} \in \mathbb{R}. \quad (37)$$

The integration constants  $e_1$ ,  $e_2$ ,  $e_4$ , and  $e_5$  are fixed by the initial condition  $G(t = t_1 = 0) = G_1 = 0$

$$\begin{aligned} e_1 &= \frac{x_1}{D_0} - \frac{(A_0 q_1)^{1/2}}{D_0^{3/2}} \arctan \left( \sqrt{\frac{D_0}{A_0 q_1}} x_1 \right) \\ e_2 &= e_4 = x_1^3 \\ e_5 &= 0, \end{aligned}$$

whereas the integration constant  $e_3$  is determined by the transition condition  $G(t = t_T^{(s)} | 0 \leq t < t_T^{(s)}) = G(t = t_T^{(s)} | t_T^{(s)} \leq t < t_2)$

$$e_3 = (3 A_0 q_1 t_T^{(s)} + x_1^3)^{1/3} - x_1 - D_0 t_T^{(s)}.$$

In the double-injection domain (DID), the solution branch  $G(t | t_2 \leq t < t_3)$  is given for  $t_2 \leq t < \min(t_3, t_T(2))$  by

- Sol.(15) for  $S_2 = \emptyset$ ,
- Sol.(22) for  $S_2 \neq \emptyset$  and  $t_2 < t_T^{(n)}(2) < t_T(2)$ ,
- Sol.(23) for  $S_2 \neq \emptyset$  and  $t_2 < t_T(2) \leq t_T^{(n)}(2)$ ,
- Sol.(24) for  $S_2 \neq \emptyset$  and  $t_T^{(n)}(2) \leq t_2$ ,

and for  $t_T(2) \leq t < t_3$  by

- Sol.(31) for  $t_T(2) < t_T^{(f)}(2) < t_3$ ,
- Sol.(32) for  $t_T(2) < t_3 \leq t_T^{(f)}(2)$ ,
- Sol.(33) for  $t_T^{(f)}(2) \leq t_T(2)$

with  $j = 2$ . The initial value  $G_2$  is fixed by requiring continuity of the SID and DID solution branches at the time of the second injection, yielding

$$G_2 = \begin{cases} G(t = t_2 | t_T^{(s)} \leq t < t_2; \text{Sol.}(35)) & \text{for } 0 < t_T^{(s)} < t_2 \\ G(t = t_2 | 0 \leq t < t_2; \text{Sol.}(36)) & \text{for } 0 < t_2 \leq t_T^{(s)} \\ G(t = t_2 | 0 \leq t < t_2; \text{Sol.}(37)) & \text{for } t_T^{(s)} \leq 0. \end{cases}$$

In addition to the initial DID updating of constants at  $t = t_2$ , we have to perform NID-FID updates at  $t = t_T(1)$  and  $t = t_T(2)$  if  $t_T(1), t_T(2) \in [t_2, t_3]$ . Assuming that both transition times are contained in this interval with the order  $t_2 < t_T(1) < t_T(2) < t_3$ , we have to update the initial DID sets  $S_1$  and  $S_2$  twice. More precisely, at the time of the second injection  $t = t_2$ , both the first and the second injection are contained in  $S_1$  while  $S_2$  is empty. During the temporal progression toward the upper bound  $t_3$ , the first injection switches from  $S_1$  to  $S_2$  at  $t = t_T(1)$ , whereas the second injection continues to be in  $S_1$ . At  $t = t_T(2)$ , also the second injection switches over to  $S_2$ , leaving  $S_1$  empty. This amounts to the following updating sequence:

- $t_2 \leq t < t_T(1)$ :  $M_1(2, S_2 = \emptyset) = D_0 + A_0 \sum_{j=1}^2 \frac{q_j}{x_j^2} \left(1 + \frac{2G_j}{x_j}\right)$ ,  $M_2(2, S_2 = \emptyset) = -2A_0 \sum_{j=1}^2 \frac{q_j}{x_j^3}$ ,  
 $N_1(2, S_2 = \emptyset) = N_2(2, S_2 = \emptyset) = 0$ , and  $P_1(2, S_2 = \emptyset) = D_0 + A_0 \sum_{j=1}^2 \frac{q_j}{x_j^2}$ ,
- $t_T(1) \leq t < t_T(2)$ :  $M_1(2, S_2 = \{1\}) = D_0 + \frac{A_0 q_2}{x_2^2} \left(1 + \frac{2G_2}{x_2}\right)$ ,  $M_2(2, S_2 = \{1\}) = -\frac{2A_0 q_2}{x_2^3}$ ,  
 $N_1(2, S_2 = \{1\}) = A_0 q_1$ ,  $N_2(2, S_2 = \{1\}) = -2A_0 q_1 x_1$ ,  
and  $P_1(2, S_2 = \{1\}) = D_0 + \frac{A_0 q_2}{x_2^2}$ ,
- $t_T(2) \leq t < t_3$ :  $M_1(2, S_2 = \{1, 2\}) = D_0$ ,  $M_2(2, S_2 = \{1, 2\}) = 0$ ,  $N_1(2, S_2 = \{1, 2\}) = A_0 \sum_{k=1}^2 q_k$ ,  
 $N_2(2, S_2 = \{1, 2\}) = 2A_0 \sum_{k=1}^2 q_k (G_k - x_k)$ , and  $P_1(2, S_2 = \{1, 2\}) = D_0$ .

Repeating this procedure for the remaining  $m - 2$  injections results in a formal representation of  $G$  for  $t : 0 \leq t < \infty$  given by

$$\begin{aligned} G(t | 0 \leq t < \infty) &= H(t) H(t_2 - t) G_{\text{SID}}(t | 0 \leq t < t_2) \\ &+ \sum_{i=2}^m H(t - t_i) H(t_{i+1} - t) H(t_T(i) - t) \left[ \chi(S_2 = \emptyset) G_{\text{NID}}(t | t_i \leq t < t_T(i); S_2 = \emptyset) \right. \\ &\quad \left. + [1 - \chi(S_2 = \emptyset)] G_{\text{NID}}(t | t_i \leq t < t_T(i); S_2 \neq \emptyset) \right] \\ &+ \sum_{i=2}^m H(t - t_T(i)) H(t_{i+1} - t) G_{\text{FID}}(t | t_T(i) \leq t < t_{i+1}), \end{aligned} \tag{38}$$

where

$$\chi(S_2 = \emptyset) := \begin{cases} 1 & \text{for } S_2 = \emptyset \\ 0 & \text{for } S_2 \neq \emptyset \end{cases}$$

is the characteristic function. The SID contribution  $G_{\text{SID}}(t | 0 \leq t < t_2)$ , both NID contributions  $G_{\text{NID}}(t | t_i \leq t < t_T(i); S_2 = \emptyset)$ ,  $G_{\text{NID}}(t | t_i \leq t < t_T(i); S_2 \neq \emptyset)$ , the FID contribution  $G_{\text{FID}}(t | t_T(i) \leq t < t_{i+1})$ , and the initial constants  $G_i$  are stated explicitly in Appendix D. Note that here the updating of constants is suppressed for readability. It could, however, be written down explicitly similar to the updating of the integration constants presented in Appendix C.

### III. SYNCHROTRON AND SSC INTENSITIES

In this section, we calculate the optically thin synchrotron intensity and the SSC intensity in the Thomson limit. The optically thick component of the synchrotron intensity is not considered because it was shown in [31] that, for all frequencies and times, it provides only a small contribution to the high-energy SSC component.

#### A. Synchrotron Intensity

The optically thin synchrotron intensity  $I_{\text{syn.}}(\epsilon, t)$  for an isotropically distributed electron number density is given by

$$I_{\text{syn.}}(\epsilon, t) = \frac{\mathcal{R}_0}{4\pi} \int_0^\infty n(\gamma, t) P(\epsilon, \gamma) d\gamma, \quad (39)$$

where the function

$$P(\epsilon, \gamma) = P_0 \frac{\epsilon}{\gamma^2} CS\left(\frac{2\epsilon}{3\epsilon_0 \gamma^2}\right) \quad (40)$$

is the pitch-angle-averaged spectral synchrotron power of a single electron in a magnetic field of normalized strength  $b$ ,  $\epsilon := E_{\text{syn.}}/(m_e c^2)$  is the normalized synchrotron photon energy,  $P_0 = 8.5 \times 10^{23} \text{ eV s}^{-1}$ , and  $\epsilon_0 := 2.3 \times 10^{-14} b$  [9]. The  $CS$  function is discussed in detail in Appendix E. Here, we employ the approximation

$$CS(z) \approx \frac{a_0}{z^{2/3} (1 + z^{1/3} \exp(z))}, \quad z \in \mathbb{R}_{\geq 0}, \quad (41)$$

where  $a_0 = 1.15$ . Substituting the electron number density (10) and the synchrotron power (40) with the  $CS$  function (41) into formula (39), we obtain for the optically thin synchrotron intensity

$$I_{\text{syn.}}(\epsilon, t) = I_{0,\text{syn.}} \epsilon^{1/3} \sum_{i=1}^m \frac{q_i H(t - t_i) \mathcal{Y}_i^{2/3}(t)}{1 + \left(\frac{2\epsilon}{3\epsilon_0}\right)^{1/3} \mathcal{Y}_i^{2/3}(t) \exp\left(\frac{2\epsilon}{3\epsilon_0} \mathcal{Y}_i^2(t)\right)} \quad (42)$$

with  $I_{0,\text{syn.}} := 3^{2/3} \mathcal{R}_0 P_0 a_0 \epsilon_0^{2/3} / (2^{8/3} \pi)$  and the abbreviation  $\mathcal{Y}_i(t) := G(t) - G_i + x_i$ . For comparisons with observational data or for generic case studies, that is, for fitting or plotting lightcurves, we have to compute the energy-integrated synchrotron intensity

$$\bar{I}_{\text{syn.}}(t; \epsilon_{\min.}, \epsilon_{\max.}) = \int_{\epsilon_{\min.}}^{\epsilon_{\max.}} I_{\text{syn.}}(\epsilon, t) d\epsilon$$

with a lower integration limit  $\epsilon_{\min.}$  corresponding to the energy of the first data point in the fluence SED and an upper integration limit  $\epsilon_{\max.}$  defined by the last. Using (42), this quantity yields

$$\bar{I}_{\text{syn.}}(t; \epsilon_{\min.}, \epsilon_{\max.}) = \left(\frac{3\epsilon_0}{2}\right)^{4/3} I_{0,\text{syn.}} \sum_{i=1}^m \frac{q_i H(t - t_i)}{\mathcal{Y}_i^2(t)} \int_{\tau_{i,\min.}}^{\tau_{i,\max.}} \frac{\tilde{\tau}^{1/3}}{1 + \tilde{\tau}^{1/3} \exp(\tilde{\tau})} d\tilde{\tau},$$

where  $\tau_{i,\min.} := 2\epsilon_{\min.} \mathcal{Y}_i^2/(3\epsilon_0)$  and  $\tau_{i,\max.} := 2\epsilon_{\max.} \mathcal{Y}_i^2/(3\epsilon_0)$ . In order to solve the integral, we approximate the integrand by  $\tilde{\tau}^{1/3}$  for  $\tilde{\tau} \leq 1$  and  $\exp(-\tilde{\tau})$  for  $\tilde{\tau} > 1$ . This is justified because the approximated  $CS$  function

(41) is only adapted to the asymptotics  $\tilde{\tau} \ll 1$  and  $\tilde{\tau} \gg 1$  of the exact  $CS$  function and extrapolated in between. Moreover, since  $\tau_{i,\min.}$  and  $\tau_{i,\max.}$  depend on the time  $t$ , we have to consider the three cases where  $1 \leq \tau_{i,\min.}$ ,  $\tau_{i,\min.} < 1 \leq \tau_{i,\max.}$ , and  $\tau_{i,\max.} < 1$ . Accordingly, the integral results in

$$\begin{aligned} \int_{\tau_{i,\min.}}^{\tau_{i,\max.}} \frac{\tilde{\tau}^{1/3}}{1 + \tilde{\tau}^{1/3} \exp(\tilde{\tau})} d\tilde{\tau} \approx & H(\tau_{i,\min.} - 1) [\exp(-\tau_{i,\min.}) - \exp(-\tau_{i,\max.})] \\ & + H(\tau_{i,\max.} - 1) H(1 - \tau_{i,\min.}) \left[ \frac{3}{4} \left( 1 - \tau_{i,\min.}^{4/3} \right) - \exp(-\tau_{i,\max.}) + \exp(-1) \right] \\ & + \frac{3}{4} H(1 - \tau_{i,\max.}) \left[ \tau_{i,\max.}^{4/3} - \tau_{i,\min.}^{4/3} \right]. \end{aligned} \quad (43)$$

## B. SSC Intensity

In the computation of the SSC intensity

$$I_{\text{SSC}}(\epsilon_s, t) = \frac{\mathcal{R}_0}{4\pi} \int_0^\infty n(\gamma, t) P_{\text{SSC}}(\epsilon_s, \gamma, t) d\gamma, \quad (44)$$

where  $P_{\text{SSC}}(\epsilon_s, \gamma, t)$  is the SSC power of a single electron and  $\epsilon_s := E_s/(m_e c^2)$  is the normalized scattered photon energy, we have to employ the Thomson limit because the SSC radiative losses in (2) are already restricted to the Thomson regime. In this limit, the SSC power reads [9, 19]

$$P_{\text{SSC}}(\epsilon_s, \gamma, t) = \frac{4}{3} \sigma_T c \gamma^2 \mathcal{E}(\epsilon_s, t)$$

with the Thomson cross section  $\sigma_T = 6.65 \times 10^{-25} \text{ cm}^2$  and the total SSC photon energy density  $\mathcal{E}(\epsilon_s, t)$ . For relativistic electrons with  $\gamma \gg 1$  and synchrotron photon energies in the Thomson regime for which  $\gamma \epsilon \ll 1$ , the characteristic energy of the SSC-scattered photons is  $\epsilon_s \approx 4\gamma^2 \epsilon$  [19], corresponding to head-on collisions of the synchrotron photons with the electrons [9, 23, 28]. Thus, it is justified to apply a monochromatic approximation in the total SSC photon energy density in form of a Dirac distribution that spikes at this characteristic energy

$$\mathcal{E}(\epsilon_s, t) = \frac{1}{4\pi} \int_0^\infty \epsilon N(\epsilon, t) \delta(\epsilon_s - 4\gamma^2 \epsilon) d\epsilon,$$

where

$$N(\epsilon, t) = \frac{4\pi I_{\text{syn.}}(\epsilon, t)}{c\epsilon}$$

is the synchrotron photon number density. We remark that by assuming an isotropic, relativistic electron distribution, the synchrotron photon number density becomes inevitably isotropically distributed. Substituting the latter formulas into (44) and using Fubini's theorem, we obtain

$$I_{\text{SSC}}(\epsilon_s, t) = \frac{\mathcal{R}_0 \sigma_T \epsilon_s}{12\pi} \int_0^\infty \frac{I_{\text{syn.}}(\epsilon, t)}{\epsilon} \int_0^{1/\epsilon} n(\gamma, t) \delta(\epsilon_s - 4\gamma^2 \epsilon) d\gamma d\epsilon, \quad (45)$$

in which the upper  $\gamma$ -integration limit arises from the restriction to the Thomson regime. With the electron number density (10) and the synchrotron intensity (42), the SSC intensity (45) yields, after having performed both integrations,

$$I_{\text{SSC}}(\epsilon_s, t) = I_{0,\text{SSC}} \epsilon_s^{1/3} \sum_{i,j=1}^m \frac{q_i q_j H(t - t_i) H(t - t_j) H\left(1 - \frac{\epsilon_s}{4} \mathcal{Y}_j(t)\right) [\mathcal{Y}_i(t) \mathcal{Y}_j(t)]^{2/3}}{1 + \left(\frac{\epsilon_s}{6\epsilon_0}\right)^{1/3} [\mathcal{Y}_i(t) \mathcal{Y}_j(t)]^{2/3} \exp\left(\frac{\epsilon_s}{6\epsilon_0} [\mathcal{Y}_i(t) \mathcal{Y}_j(t)]^2\right)}, \quad (46)$$

where  $I_{0,\text{SSC}} := \mathcal{R}_0 \sigma_T I_{0,\text{syn.}}/(2^{2/3} 12\pi)$ . The double sum, with the index  $i$  referring to the  $i$ th synchrotron photon population and the index  $j$  to the  $j$ th electron population, accounts for all combinations of SSC scattering

between the various electron and synchrotron photon populations. For the corresponding energy-integrated SSC intensity, we find

$$\begin{aligned} \bar{I}_{\text{SSC}}(t; \epsilon_{\text{s,min.}}, \epsilon_{\text{s,max.}}) &= (6\epsilon_0)^{4/3} I_{0,\text{SSC}} \sum_{i,j=1}^m \frac{q_i q_j H(t-t_i) H(t-t_j)}{[\mathcal{Y}_i(t) \mathcal{Y}_j(t)]^2} \\ &\times \int_{\tau_{ij,\text{min.}}}^{\min(\tau_{ij,\text{max.}}, 2\mathcal{Y}_i^2 \mathcal{Y}_j / (3\epsilon_0))} \frac{\tilde{\tau}^{1/3}}{1 + \tilde{\tau}^{1/3} \exp(\tilde{\tau})} d\tilde{\tau}, \end{aligned}$$

where  $\tau_{ij,\text{min.}} := \epsilon_{\text{s,min.}} (\mathcal{Y}_i \mathcal{Y}_j)^2 / (6\epsilon_0)$  and  $\tau_{ij,\text{max.}} := \epsilon_{\text{s,max.}} (\mathcal{Y}_i \mathcal{Y}_j)^2 / (6\epsilon_0)$ . The integral is given by (43), however, with adapted integration limits.

#### IV. SYNCHROTRON AND SSC FLUENCES

We compute the total fluences associated with the synchrotron intensity (42) and the SSC intensity (46). For this purpose, we derive a general expression for the total fluence that, on the one hand, employs the function  $G$  and, on the other hand, explicitly displays the various approximate cases of the Jacobian determinant of the integration measure. For simplicity, the updating of constants is once more suppressed. With  $(\varepsilon, I, F) \in \{(\epsilon, I_{\text{syn.}}, F_{\text{syn.}}), (\epsilon_{\text{s}}, I_{\text{SSC}}, F_{\text{SSC}})\}$ , the total fluence  $F$  is given by

$$F(\varepsilon) = \int_0^\infty I(\varepsilon, t) dt = \sum_{i=1}^m \int_{G_i}^{G_{i+1}} I(\varepsilon, G) \frac{dt}{dG} dG. \quad (47)$$

By means of Eqs.(34), (14), (16), and (25), the Jacobian determinant yields

$$\frac{dt}{dG} = \begin{cases} \frac{(G+x_1)^2}{D_0(G+x_1)^2 + A_0 q_1} & \text{for } 0 \leq G < G_2 \\ \frac{1}{M_1(i) + M_2(i) G} & \text{for } G_i \leq G < \min(G_{i+1}, G_T(i)) \text{ and } S_2 = \emptyset \\ \frac{G^2}{P_1(i) G^2 + N_1(i)} & \text{for } G_i \leq G < \min(G_{i+1}, G_T(i)) \text{ and } S_2 \neq \emptyset \\ \frac{G^3}{D_0 G^3 + N_1(i) G + N_2(i)} & \text{for } \min(G_{i+1}, G_T(i)) \leq G < G_{i+1}, \end{cases} \quad (48)$$

where  $i: 2 \leq i \leq m$ . Substituting (48) into (47), we obtain the expression

$$\begin{aligned} F(\varepsilon) &= \int_0^{G_2} \frac{I(\varepsilon, G) (G+x_1)^2}{D_0 (G+x_1)^2 + A_0 q_1} dG + \sum_{i=2}^m \chi(S_2 = \emptyset) \int_{G_i}^{\min(G_{i+1}, G_T(i))} \frac{I(\varepsilon, G)}{M_1(i) + M_2(i) G} dG \\ &+ \sum_{i=2}^m [1 - \chi(S_2 = \emptyset)] \int_{G_i}^{\min(G_{i+1}, G_T(i))} \frac{I(\varepsilon, G) G^2}{P_1(i) G^2 + N_1(i)} dG \\ &+ \sum_{i=2}^m \int_{\min(G_{i+1}, G_T(i))}^{G_{i+1}} \frac{I(\varepsilon, G) G^3}{D_0 G^3 + N_1(i) G + N_2(i)} dG. \end{aligned} \quad (49)$$

In the following, only the second integral of (49) is calculated in detail for both the synchrotron and the SSC case. The remaining integrals can be solved accordingly. Note that the first and the third integral are special cases of the fourth integral for  $N_2 \equiv 0$  and suitably adapted constants and integration limits.

### A. Synchrotron Fluence

With  $I = I_{\text{syn.}}(\epsilon, G)$  according to (42), the second integral of (49) reads

$$\begin{aligned} \mathcal{J}_{2,i,\text{syn.}}(\epsilon) &:= \int_{G_i}^{\min(G_{i+1}, G_T(i))} \frac{I_{\text{syn.}}(\epsilon, G)}{M_1(i) + M_2(i) G} dG \\ &= I_{0,\text{syn.}} \epsilon^{1/3} \sum_{l=1}^i q_l \int_{G_i}^{\min(G_{i+1}, G_T(i))} \frac{[M_1(i) + M_2(i) G]^{-1} \mathcal{Y}_l^{2/3}(G)}{1 + \left(\frac{2\epsilon}{3\epsilon_0}\right)^{1/3} \mathcal{Y}_l^{2/3}(G) \exp\left(\frac{2\epsilon}{3\epsilon_0} \mathcal{Y}_l^2(G)\right)} dG. \end{aligned}$$

Using  $\tau_l := 2\epsilon \mathcal{Y}_l^2/(3\epsilon_0)$  and, since  $M_1(i) \gg M_2(i) G$ , approximating the Jacobian determinant by

$$[M_1(i) + M_2(i) G]^{-1} = \frac{1}{M_1(i)} \sum_{n=0}^{\infty} \left(-\frac{M_2(i) G}{M_1(i)}\right)^n \approx \frac{1}{M_1(i)} \left(1 - \frac{M_2(i) G}{M_1(i)}\right)$$

gives

$$\begin{aligned} \mathcal{J}_{2,i,\text{syn.}}(\epsilon) &= \frac{(3\epsilon_0)^{5/6} I_{0,\text{syn.}}}{2^{11/6}} \epsilon^{-1/2} \sum_{l=1}^i q_l \int_{\tau_l(G_i)}^{\tau_l(\min(G_{i+1}, G_T(i)))} \frac{1}{M_1(i)} \left[1 - \frac{M_2(i)}{M_1(i)} \left(\sqrt{\frac{3\epsilon_0 \tilde{\tau}}{2\epsilon}} + G_l - x_l\right)\right] \\ &\quad \times \frac{d\tilde{\tau}}{\tilde{\tau}^{1/6} (1 + \tilde{\tau}^{1/3} \exp(\tilde{\tau}))}. \end{aligned} \quad (50)$$

Similar to the evaluation of the energy-integrated intensities (cf. the paragraph directly above formula (43)), we approximate the integrand for  $\tilde{\tau} \leq 1$  by

$$\left[1 - \frac{M_2(i)}{M_1(i)} (G_l - x_l)\right] \tilde{\tau}^{-1/6} - \frac{M_2(i)}{M_1(i)} \sqrt{\frac{3\epsilon_0}{2\epsilon}} \tilde{\tau}^{1/3}$$

and for  $\tilde{\tau} > 1$  by

$$\left(\left[1 - \frac{M_2(i)}{M_1(i)} (G_l - x_l)\right] \tilde{\tau}^{-1/2} - \frac{M_2(i)}{M_1(i)} \sqrt{\frac{3\epsilon_0}{2\epsilon}}\right) \exp(-\tilde{\tau}).$$

Thus, (50) is solved approximately by

$$\begin{aligned} \mathcal{J}_{2,i,\text{syn.}}(\epsilon) &\approx \frac{(3\epsilon_0)^{5/6} I_{0,\text{syn.}}}{2^{11/6}} \epsilon^{-1/2} \sum_{l=1}^i \frac{q_l}{M_1(i)} \left[ H(\tau_l(G_i) - 1) \mathcal{A}_{l,1}(\epsilon) \right. \\ &\quad \left. + H\left(\tau_l(\min(G_{i+1}, G_T(i))) - 1\right) H(1 - \tau_l(G_i)) \mathcal{A}_{l,2}(\epsilon) + H\left(1 - \tau_l(\min(G_{i+1}, G_T(i)))\right) \mathcal{A}_{l,3}(\epsilon) \right] \end{aligned}$$

with

$$\begin{aligned} \mathcal{A}_{l,1}(\epsilon) &:= \left[1 - \frac{M_2(i)}{M_1(i)} (G_l - x_l)\right] \Gamma\left(\frac{1}{2}, \tau_l(G_i), \tau_l(\min(G_{i+1}, G_T(i)))\right) \\ &\quad + \frac{M_2(i)}{M_1(i)} \sqrt{\frac{3\epsilon_0}{2\epsilon}} \left[\exp\left(-\tau_l(\min(G_{i+1}, G_T(i)))\right) - \exp(-\tau_l(G_i))\right] \\ \mathcal{A}_{l,2}(\epsilon) &:= \left[1 - \frac{M_2(i)}{M_1(i)} (G_l - x_l)\right] \left[\Gamma\left(\frac{1}{2}, 1, \tau_l(\min(G_{i+1}, G_T(i)))\right) + \frac{6}{5} (1 - \tau_l^{5/6}(G_i))\right] \\ &\quad + \frac{M_2(i)}{M_1(i)} \sqrt{\frac{3\epsilon_0}{2\epsilon}} \left[\exp\left(-\tau_l(\min(G_{i+1}, G_T(i)))\right) - \frac{3}{4} (1 - \tau_l^{4/3}(G_i)) - \exp(-1)\right] \end{aligned}$$

$$\begin{aligned} \mathcal{A}_{l,3}(\epsilon) &:= \frac{6}{5} \left[ 1 - \frac{M_2(i)}{M_1(i)} (G_l - x_l) \right] [\tau_l^{5/6}(\min(G_{i+1}, G_T(i))) - \tau_l^{5/6}(G_i)] \\ &\quad - \frac{3^{3/2} M_2(i)}{2^{5/2} M_1(i)} \sqrt{\frac{\epsilon_0}{\epsilon}} [\tau_l^{4/3}(\min(G_{i+1}, G_T(i))) - \tau_l^{4/3}(G_i)] \end{aligned}$$

and the generalized incomplete gamma function defined for  $a \in \mathbb{C}$  and  $\text{Re}(a) > 0$  by [1]

$$\Gamma(a, y, z) := \int_y^z t^{a-1} \exp(-t) dt.$$

In the special case  $a = 1/2$ , the generalized incomplete gamma function can be expressed in terms of the error function, namely  $\Gamma(1/2, y, z) = \sqrt{\pi} [\text{erf}(z) - \text{erf}(y)]$ .

## B. SSC Fluence

With  $I = I_{\text{SSC}}(\epsilon_s, G)$  given in (46), the second integral of (49) becomes

$$\begin{aligned} \mathcal{J}_{2,i,\text{SSC}}(\epsilon_s) &:= \int_{G_i}^{\min(G_{i+1}, G_T(i))} \frac{I_{\text{SSC}}(\epsilon_s, G)}{M_1(i) + M_2(i) G} dG \\ &= I_{0,\text{SSC}} \epsilon_s^{1/3} \sum_{k,l=1}^i q_k q_l H\left(\frac{4}{\epsilon_s} - G_i + G_l - x_l\right) \\ &\quad \times \int_{G_i}^{\min(G_{i+1}, G_T(i), 4/\epsilon_s + G_l - x_l)} \frac{[M_1(i) + M_2(i) G]^{-1} [\mathcal{Y}_k(G) \mathcal{Y}_l(G)]^{2/3}}{1 + \left(\frac{\epsilon_s}{6\epsilon_0}\right)^{1/3} [\mathcal{Y}_k(G) \mathcal{Y}_l(G)]^{2/3} \exp\left(\frac{\epsilon_s}{6\epsilon_0} [\mathcal{Y}_k(G) \mathcal{Y}_l(G)]^2\right)} dG. \end{aligned} \quad (51)$$

An approximate analytical solution of this integral can be derived with the same method as in the case of the synchrotron fluence. However, one could also employ the methods used for the computation of the NID-FID transition time, which are explained in more detail in Appendix B, as follows. For the mean-value-theorem method, we first define the function

$$\mathcal{H}_{kl}(\epsilon_s, G) := \frac{[\mathcal{Y}_k(G) \mathcal{Y}_l(G)]^{2/3}}{1 + \left(\frac{\epsilon_s}{6\epsilon_0}\right)^{1/3} [\mathcal{Y}_k(G) \mathcal{Y}_l(G)]^{2/3} \exp\left(\frac{\epsilon_s}{6\epsilon_0} [\mathcal{Y}_k(G) \mathcal{Y}_l(G)]^2\right)}.$$

Since  $\mathcal{H}_{kl}(\epsilon_s, G) \in C^\infty(\mathbb{R}_{\geq 0}^2)$  and  $[M_1(i) + M_2(i) G]^{-1}$  is positive and integrable, we can apply the first mean value theorem for integration in (51). Thus, there exists a number  $\xi_{il} \in [G_i, \min(G_{i+1}, G_T(i), 4/\epsilon_s + G_l - x_l)]$  such that

$$\begin{aligned} \mathcal{J}_{2,i,\text{SSC}}(\epsilon_s) &= I_{0,\text{SSC}} \epsilon_s^{1/3} \sum_{k,l=1}^i q_k q_l H\left(\frac{4}{\epsilon_s} - G_i + G_l - x_l\right) \mathcal{H}_{kl}(\epsilon_s, \xi_{il}) \\ &\quad \times \int_{G_i}^{\min(G_{i+1}, G_T(i), 4/\epsilon_s + G_l - x_l)} \frac{dG}{M_1(i) + M_2(i) G}. \end{aligned}$$

Choosing the midpoint of the integration interval as an approximate value for  $\xi_{il}$  yields

$$\begin{aligned} \mathcal{J}_{2,i,\text{SSC}}(\epsilon_s) &\approx I_{0,\text{SSC}} \epsilon_s^{1/3} \sum_{k,l=1}^i \frac{q_k q_l}{M_2(i)} H\left(\frac{4}{\epsilon_s} - G_i + G_l - x_l\right) \mathcal{H}_{kl}\left(\epsilon_s, \frac{G_i + \min(G_{i+1}, G_T(i), 4/\epsilon_s + G_l - x_l)}{2}\right) \\ &\quad \times \ln(M_1(i) + M_2(i) G) \Big|_{G_i}^{\min(G_{i+1}, G_T(i), 4/\epsilon_s + G_l - x_l)}. \end{aligned}$$



The trapezoid-approximation method on the other hand results in the expression

$$\mathcal{I}_{2,i,\text{SSC}}(\epsilon_s) \approx I_{0,\text{SSC}} \epsilon_s^{1/3} \sum_{k,l=1}^i q_k q_l H\left(\frac{4}{\epsilon_s} - G_i + G_l - x_l\right) \frac{\min(G_{i+1}, G_T(i), 4/\epsilon_s + G_l - x_l) - G_i}{2} \\ \times \left[ \frac{\mathcal{H}_{kl}(\epsilon_s, G_i)}{M_1(i) + M_2(i) G_i} + \frac{\mathcal{H}_{kl}(\epsilon_s, \min(G_{i+1}, G_T(i), 4/\epsilon_s + G_l - x_l))}{M_1(i) + M_2(i) \min(G_{i+1}, G_T(i), 4/\epsilon_s + G_l - x_l)} \right].$$

## V. LIGHTCURVES AND FLUENCE SEDS

To obtain realistic lightcurves, we have to consider injections of finite duration time and radiative transport inside the emission region. But since, for reasons of computational feasibility, we have only employed Dirac distributions for the time profile of our source function and did not concern ourselves with any details of radiative transport, we have to mimic both by modeling each flare via a sequence of suitably distributed, instantaneous injections. In more detail, we partition the  $i$ th flare into  $n_i$  separate injections labeled by a subscript  $p \in \{1, \dots, n_i\}$ , which are induced equidistantly over the entire emission region given by  $2\mathcal{R}_0$ , i.e., the  $p$ th injection of the  $i$ th flare occurs at the time  $t_i + \kappa_{ip}$  with

$$\kappa_{ip} := \frac{p-1}{n_i-1} \frac{2\mathcal{R}_0}{c},$$

and for each of which we use the quantities derived in Section III. Thus, we find for the energy-integrated synchrotron intensity

$$\bar{\mathcal{I}}_{\text{syn.}}(t; \epsilon_{\min.}, \epsilon_{\max.}) = \int_{\epsilon_{\min.}}^{\epsilon_{\max.}} \mathcal{I}_{\text{syn.}}(\epsilon, t) d\epsilon = \int_{\epsilon_{\min.}}^{\epsilon_{\max.}} \sum_{i=1}^m \sum_{p=1}^{n_i} q_i(p) H(t - t_i - \kappa_{ip}) I_{ip}(\epsilon, t) d\epsilon, \quad (52)$$

where  $(q_i(p))_{p \in \{1, \dots, n_i\}}$  for all  $i : 1 \leq i \leq m$  is a specific distribution satisfying the constraint

$$q_i = \sum_{p=1}^{n_i} q_i(p) \quad (53)$$

and the function  $I_{ip}$  is, according to the original synchrotron intensity (42), defined by

$$I_{ip}(\epsilon, t) := \frac{I_{0,\text{syn.}} \epsilon^{1/3} \mathcal{Y}_{ip}^{2/3}(t)}{1 + \left(\frac{2\epsilon}{3\epsilon_0}\right)^{1/3} \mathcal{Y}_{ip}^{2/3}(t) \exp\left(\frac{2\epsilon}{3\epsilon_0} \mathcal{Y}_{ip}^2(t)\right)}$$

with  $\mathcal{Y}_{ip}(t) := G(t) - G(t_i + \kappa_{ip}) + x_i$ . Similarly, we can construct a proper formula for the energy-integrated SSC intensity. We refrain from showing a parameter study for lightcurves because an adequate value for  $n_i$ , which is at least of the order  $\mathcal{O}(10^4)$ , results in numerical computations that would exceed our available CPU time by far. For the associated total fluence SEDs, it is an entirely different matter as we can illustrate their functional shapes using their suprema given by the special case  $n_i = 1$  for all  $i : 1 \leq i \leq m$ , in which each flare is modeled by a single injection (cf. Section IV). In the following, we show by direct calculation that the supremum of the total fluence of the synchrotron intensity  $\mathcal{I}_{\text{syn.}}(\epsilon, t)$  defined in (52) indeed coincides, up to a constant factor, with the total fluence of this special case. To this end, we substitute  $\mathcal{I}_{\text{syn.}}(\epsilon, t)$  into the expression for the total fluence and employ the variable  $G$ , resulting in

$$\mathcal{F}_{\text{syn.}}(\epsilon) = \int_0^\infty \mathcal{I}_{\text{syn.}}(\epsilon, t) dt = \sum_{i=1}^m \sum_{p=1}^{n_i} q_i(p) \int_{t_i + \kappa_{ip}}^\infty I_{ip}(\epsilon, t) dt = \sum_{i=1}^m \sum_{p=1}^{n_i} q_i(p) \int_{G(t_i + \kappa_{ip})}^\infty I_{ip}(\epsilon, G) \frac{dt}{dG} dG. \quad (54)$$

From Eq.(11), it can be deduced that the Jacobian determinant is positive and bounded

$$\left(D_0 + A_0 \sum_{i=1}^j \frac{q_i}{x_i^2}\right)^{-1} \leq \frac{dt}{dG} \leq \frac{1}{D_0},$$

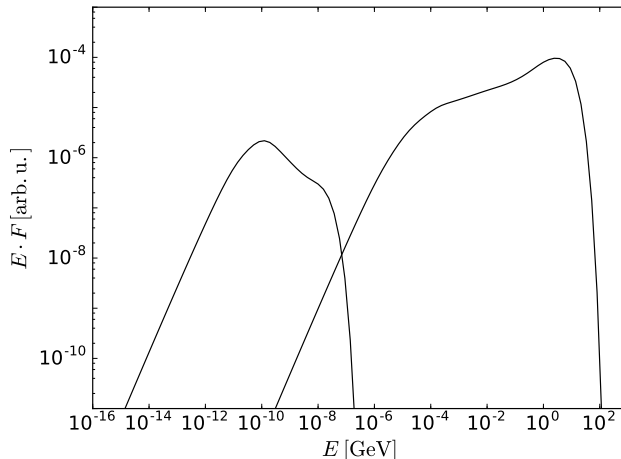


FIG. 1: Total synchrotron (left curve) and SSC (right curve) fluence SEDs for a generic three-flare scenario with parameter values  $b = 1$ ,  $D_0 = 1.3 \times 10^{-9} \text{ s}^{-1}$ ,  $A_0 = 1.2 \times 10^{-18} \text{ cm}^3 \text{ s}^{-1}$ ,  $(t_i)_{i=1,\dots,3} = (0, 1.5, 3) 2\mathcal{R}_0/c$ ,  $(q_i)_{i=1,\dots,3} = (1.5 \times 10^5, 2 \times 10^5, 5 \times 10^4) \text{ cm}^{-3}$ ,  $(x_i)_{i=1,\dots,3} = (10^{-4}, 10^{-4}, 10^{-4})$ , and  $D = 10$ .

and since  $I_{ip}$  is non-negative, we can bound the fluence (54) from above by

$$\mathcal{F}_{\text{syn.}}(\epsilon) \leq \frac{1}{D_0} \sum_{i=1}^m \sum_{p=1}^{n_i} q_i(p) \int_{G(t_i + \kappa_{ip})}^{\infty} I_{ip}(\epsilon, G) dG.$$

Then, applying the transformation  $\tilde{G}_{ip} := G - G(t_i + \kappa_{ip}) + G_i$  yields

$$\mathcal{F}_{\text{syn.}}(\epsilon) \leq \frac{1}{D_0} \sum_{i=1}^m \sum_{p=1}^{n_i} q_i(p) \int_{G_i}^{\infty} I_{ip}(\epsilon, \tilde{G}_{ip}) d\tilde{G}_{ip}.$$

Because the integral has the same value for fixed  $i$  and arbitrary  $p$ , we can always drop the subscript  $p$ . Hence, by means of the constraint (53), we obtain

$$\mathcal{F}_{\text{syn.}}(\epsilon) \leq \frac{1}{D_0} \sum_{i=1}^m \left( \sum_{p=1}^{n_i} q_i(p) \right) \int_{G_i}^{\infty} I_i(\epsilon, \tilde{G}_i) d\tilde{G}_i = \frac{1}{D_0} \sum_{i=1}^m q_i \int_{t_i}^{\infty} I_i(\epsilon, t) dt = \frac{F_{\text{syn.}}(\epsilon)}{D_0}, \quad (55)$$

proving the claim. In Figure 1, we plot the total synchrotron and SSC fluence SEDs for a generic three-flare, SSC-dominated scenario, in which each flare is modeled by a single injection according to (55), using a set of realistic blazar parameter values. The resulting functional shapes indicate that our model can reproduce the typical fluence SED behavior of blazars visible in observational data.

## VI. SUMMARY AND OUTLOOK

We introduced a fully analytical, time-dependent leptonic one-zone model for the flaring of blazars that employs combined synchrotron and SSC radiative losses of multiple relativistic electron populations. More precisely, we derived an approximate analytical solution of the relativistic transport equation of the volume-averaged differential electron number density for several successively and instantaneously injected, mono-energetic, spatially isotropically distributed, interacting electron populations, which are subjected to linear, time-independent synchrotron radiative losses and nonlinear, time-dependent SSC radiative losses in the Thomson limit. Using this solution, we computed the optically thin synchrotron intensity, the SSC intensity in the Thomson limit, as well as the corresponding total fluences. Moreover, we mimicked finite injection durations and radiative transport by modeling flares in terms of sequences of instantaneous injections. Finally, we plotted generic total synchrotron and SSC fluence SEDs for a set of suitable parameter values, showing that the model can reproduce their characteristic broad-band shapes, which are seen in observational data. We point out that the SSC radiative loss term considered here is strictly valid only in the Thomson regime. Nonetheless, it can be generalized to include the full Klein-Nishina cross section. This leads to a model for which similar yet technically more involved methods apply.

Further, in order to make our simple analytical model more realistic, terms accounting for spatial diffusion and for electron escape could be added to the transport equation. Also, more elaborate source functions, e.g., with a power law energy dependence, a time dependence in form of rectangular functions for finite injection durations, and with a proper spatial dependence may be considered. However, judging from the complexity of our more elementary analysis, this is most likely only possible via numerical evaluation.

### Acknowledgments

The authors are grateful to Horst Fichtner, Reinhard Schlickeiser, and Michael Zacharias for useful discussions and comments.

### Appendix A: Laplace Method

We derive the solution  $R(x, G)$  of the PDE (6) by using a composition of two Laplace transformations. First, applying a Laplace transformation with respect to the inverse energy  $x$

$$\mathcal{L}_w(x) [\cdot] := \int_0^\infty [\cdot] \exp(-w x) dx$$

to Eq.(6) gives

$$\int_0^\infty \frac{\partial R}{\partial G} \exp(-w x) dx + \int_0^\infty \frac{\partial R}{\partial x} \exp(-w x) dx = \sum_{i=1}^m q_i \delta(G - G_i) \int_0^\infty \delta(x - x_i) \exp(-w x) dx.$$

Evaluating the second integral on the left-hand side via integration by parts and employing the Laplace transform of  $R$

$$K(w, G) := \int_0^\infty R(x, G) \exp(-w x) dx, \quad (\text{A1})$$

we obtain

$$\frac{\partial K}{\partial G} + R \exp(-w x)|_{x \rightarrow \infty} - R(0, G) + w K = \sum_{i=1}^m q_i \delta(G - G_i) \exp(-w x_i) [H(x - x_i)|_{x \rightarrow \infty} - H(x - x_i)|_{x=0}]$$

and, hence,

$$\frac{\partial K}{\partial G} - R(0, G) + w K = \sum_{i=1}^m q_i \delta(G - G_i) \exp(-w x_i). \quad (\text{A2})$$

As the normalized initial electron energies are finite and bounded from above by  $\gamma_i < 1.9 \times 10^4 b^{-1/3}$  for all  $i : 1 \leq i \leq m$  (due to the restriction to the Thomson regime) and only radiation loss processes are considered, we know that the electron number density has support

$$\text{supp } n(\gamma, t) = \{(\gamma, t) \in \mathbb{R}_{\geq 0}^2 \mid \gamma \leq \gamma_{\max.} \text{ with } \gamma_{\max.} := \max\{\gamma_i \mid 1 \leq i \leq m\}\}.$$

Thus, we can write  $n(\gamma, t) = H(\gamma_{\max.} - \gamma) n(\gamma, t)$ , yielding for the second term

$$R(0, G) = \lim_{x \searrow 0} \left( H(x - x_{\max.}) \frac{n(x, G)}{x^2} \right) = 0,$$

where  $x_{\max.} := 1/\gamma_{\max.}$ . Accordingly, Eq.(A2) becomes

$$\frac{\partial K}{\partial G} + w K = \sum_{i=1}^m q_i \delta(G - G_i) \exp(-w x_i). \quad (\text{A3})$$

Secondly, applying a Laplace transformation with respect to the function  $G$

$$\mathcal{L}_s(G) [\cdot] := \int_0^\infty [\cdot] \exp(-s G) dG$$

to Eq.(A3) results in

$$\int_0^\infty \frac{\partial K}{\partial G} \exp(-s G) dG + w \int_0^\infty K \exp(-s G) dG = \sum_{i=1}^m q_i \exp(-w x_i) \int_0^\infty \delta(G - G_i) \exp(-s G) dG. \quad (\text{A4})$$

This Laplace transformation implies that  $G$  is non-negative. With the Laplace transform of  $K$

$$M(w, s) := \int_0^\infty K(w, G) \exp(-s G) dG$$

and integration by parts as before, Eq.(A4) reads

$$K \exp(-s G)|_{G \rightarrow \infty} - K(w, 0) + (w + s) M = \sum_{i=1}^m q_i \exp(-(w x_i + s G_i)) \times [H(G - G_i)|_{G \rightarrow \infty} - H(G - G_i)|_{G=0}].$$

Since the Heaviside functions are not well-defined at the jump discontinuities at  $G = G_i$  for  $i : 1 \leq i \leq m$ , this equation reduces to

$$-K(w, 0) + (w + s) M = \sum_{i=1}^m q_i \exp(-(w x_i + s G_i)) - q_1 \exp(-w x_1) H(G)|_{G=0}, \quad (\text{A5})$$

containing an unspecified contribution in the last term on the right-hand side. At  $G = 0$ , no energy losses have yet occurred. Therefore, the electron number density is of the form  $n(x, 0) = n_1 \delta(x - x_1)$ , where  $n_1 = q_1 x_1^2$ . Substituting this density into (A1) by employing the relation  $R(x, G) = n(x, G)/x^2$ , we find

$$K(w, 0) = n_1 \int_0^\infty \frac{\exp(-w x)}{x^2} \delta(x - x_1) dx = q_1 \exp(-w x_1).$$

Choosing  $H(G)|_{G=0} = 1$ , we can use this function in order to compensate the last term on the right-hand side of Eq.(A5), yielding

$$M(w, s) = \frac{1}{w + s} \sum_{i=1}^m q_i \exp(-(w x_i + s G_i)).$$

We point out that both  $M$  and the sum are positive. Hence,  $s > -w$ , which allows us to apply the inverse Laplace transformations with respect to the variables  $s$  and  $w$  to  $M$ . This gives the solution of Eq.(6)

$$\begin{aligned} R(x, G) &= \mathcal{L}_w^{-1}(x) \mathcal{L}_s^{-1}(G) M(w, s) = \mathcal{L}_w^{-1}(x) \sum_{i=1}^m q_i H(G - G_i) \exp(-w(G - G_i + x_i)) \\ &= \sum_{i=1}^m q_i H(G - G_i) \delta(x - x_i - G + G_i). \end{aligned}$$

## Appendix B: NID-FID Transition Time

In the following, we present two different methods for the determination of the transition time  $t_T(j)$ . It is advantageous to start from the integral equation representation of the ODE (11) evaluated at the transition point  $G_T(j) = G_j + x_j$

$$t_T(j) = \int_{G_j}^{G_j + x_j} J^{-1}(\tilde{G}) d\tilde{G} \quad \text{with} \quad J^{-1}(\tilde{G}) := \frac{1}{J(\tilde{G})} = \left( D_0 + A_0 \sum_{i=1}^j \frac{q_i}{(\tilde{G} - G_i + x_i)^2} \right)^{-1}. \quad (\text{B1})$$

With  $J^{-1} \in C^\infty(\mathbb{R}_{\geq 0})$ , the first method applies the first mean value theorem for integration. Thus, there exists a point  $\xi_j \in [G_j, G_j + x_j]$  such that the transition time (B1) can be written as

$$t_T = x_j J^{-1}(\xi_j).$$

Because the mean value theorem is merely an existence theorem, we approximate the value of  $\xi_j$  by means of an additional input. Since  $J^{-1}$  is strictly increasing, a suitable choice for  $\xi_j$  is the midpoint  $G_j + x_j/2$  of the integration interval. The second method employs a trapezoid approximation. Again due to the strictly increasing functional shape of  $J^{-1}$ , the integral in (B1) can be approximated by the area  $A(j)$  of a trapezoid, which is computed as the sum of the area  $A_r(j)$  of the rectangle defined by the distance between the endpoints  $G_j$  and  $G_j + x_j$  and the height  $J^{-1}(G_j)$

$$A_r = x_j J^{-1}(G_j)$$

and the area  $A_t(j)$  of the right-angled triangle with one cathetus given by the distance between the endpoints and the other one by the height  $J^{-1}(G_j + x_j) - J^{-1}(G_j)$

$$A_t = \frac{x_j}{2} (J^{-1}(G_j + x_j) - J^{-1}(G_j)).$$

This leads to the formula

$$t_T = \frac{x_j}{2} (J^{-1}(G_j) + J^{-1}(G_j + x_j))$$

for the transition time. To obtain a more accurate approximation, one could use additional supporting points in the interval  $[G_j, G_j + x_j]$ , giving rise to a finer trapezoid decomposition of the integral. Note that in the present study, the trapezoid method yields a better approximation of the transition time.

### Appendix C: Constants of Integration – Initial and Transition Conditions and Updating

The constants of integration  $c_4, \dots, c_7$  of the NID (see (22)-(24)) and  $d_2, \dots, d_5$  of the FID (see (31)-(33)) are determined. The NID constants of integration  $c_4$ ,  $c_6$ , and  $c_7$  are fixed via the initial condition  $G(t = t_j) = G_j$ , whereas  $c_5$  is fixed via the transition condition  $G(t = t_T^{(n)}(j) | t_j \leq t < t_T^{(n)}(j)) = G(t = t_T^{(n)}(j) | t_T^{(n)}(j) \leq t < t_T(j))$ . The initial condition provides continuity of  $G$  at the transition from the  $(j-1)$ th injection domain to the  $j$ th injection domain at  $t = t_j$  and the transition condition between the nonlinear and linear NID solution branches at  $t = t_T^{(n)}(j)$ . The FID constants of integration  $d_2$ ,  $d_4$ , and  $d_5$  are specified by the initial condition  $G(t = t_T(j)) = G_T(j)$  and  $d_3$  by the transition condition  $G(t = t_T^{(f)}(j) | t_j \leq t < t_T^{(f)}(j)) = G(t = t_T^{(f)}(j) | t_T^{(f)}(j) \leq t < t_{j+1})$ . These conditions guarantee continuity between the NID and FID solution branches at  $t = t_T(j)$  and between the nonlinear and linear FID solution branches at  $t = t_T^{(f)}(j)$ , respectively. Further, the NID constants of integration have to be updated if there are  $t_T(i) \in [t_j, \min(t_{j+1}, t_T(j))]$  for  $i \in \{1, \dots, j-1\}$ , as elements of  $S_1$  switch over to  $S_2$ . Because these updates cause shifts in the NID transition time  $t_T^{(n)}$  towards larger values, we have to account for updating conditions that cover the change of order  $t_T^{(n)}(j) \leftrightarrow \min(t_{j+1}, t_T(j))$ . Below, the determination of the NID constant of integration  $c_4$  is shown in detail. The remaining constants of integration are computed accordingly. Applying the initial condition  $G(t = t_j | t_j \leq t < t_T^{(n)}(j)) = G_j$  to the first branch of (22), we obtain

$$c_4(j) = G_j^3 - 3 N_1(j) t_j.$$

The conditions – and the updated constants – for an NID-FID transition of the  $(i < j)$ th injection at  $t_j \leq t = t_T(i) < \min(t_{j+1}, t_T^{(n)}(j))$  are:

- first branch Sol.(22)  $\rightarrow$  first branch Sol.(22)

$$G(t = t_T(i) | t_j \leq t < t_T^{(n)}(j; S_2 \setminus \{i\})) = G(t = t_T(i) | t_j \leq t < t_T^{(n)}(j; S_2 \cup \{i\}))$$

$$c_4(j; S_2 \cup \{i\}) = 3 \left( N_1(j; S_2 \setminus \{i\}) - N_1(j; S_2 \cup \{i\}) \right) t_T(i) + c_4(j; S_2 \setminus \{i\})$$

- first branch Sol.(22)  $\rightarrow$  Sol.(23)

$$G(t = t_T(i) | t_j \leq t < t_T^{(n)}(j; S_2 \setminus \{i\})) = G(t = t_T(i) | t_j \leq t < t_T(j; S_2 \cup \{i\}))$$

$$c_6(j; S_2 \cup \{i\}) = 3 \left( N_1(j; S_2 \setminus \{i\}) - N_1(j; S_2 \cup \{i\}) \right) t_T(i) + c_4(j; S_2 \setminus \{i\}).$$

Since  $S_2 \cup \{i\} \neq \emptyset$  and  $t_T^{(n)}(j; S_2 \setminus \{i\}) < t_T^{(n)}(j; S_2 \cup \{i\})$ , it is obvious that transitions from the first branch of (22) to (15), from the first to the second branch of (22), and from the first branch of (22) to (24) are not possible.

#### Appendix D: Components of $G(t|0 \leq t < \infty)$ and Initial Values $G_i$

We state the implicit expressions for the SID, NID, and FID components of (38). First, the SID component is given by

$$\begin{aligned} G_{\text{SID}}(t|0 \leq t < t_2) &= H(t_T^{(s)}) \left[ H(t_2 - t_T^{(s)}) \left[ H(t_T^{(s)} - t) G(t|0 \leq t < t_T^{(s)}; \text{Sol.}(35)) \right. \right. \\ &\quad \left. \left. + H(t - t_T^{(s)}) G(t|t_T^{(s)} \leq t < t_2; \text{Sol.}(35)) \right] + H(t_T^{(s)} - t_2) G(t|0 \leq t < t_2; \text{Sol.}(36)) \right] \\ &\quad + H(-t_T^{(s)}) G(t|0 \leq t < t_2; \text{Sol.}(37)). \end{aligned}$$

For the NID component, we have to consider the two cases  $S_2 = \emptyset$  and  $S_2 \neq \emptyset$ . They yield

$$G_{\text{NID}}(t|t_i \leq t < t_T(i); S_2 = \emptyset) = G(t|t_i \leq t < t_T(i); \text{Sol.}(15))$$

and

$$\begin{aligned} G_{\text{NID}}(t|t_i \leq t < t_T(i); S_2 \neq \emptyset) &= H(t_T^{(n)}(i) - t_i) \left[ H(t_T(i) - t_T^{(n)}(i)) \right. \\ &\quad \times \left[ H(t_T^{(n)}(i) - t) G(t|t_i \leq t < t_T^{(n)}(i); \text{Sol.}(22)) + H(t - t_T^{(n)}(i)) G(t|t_T^{(n)}(i) \leq t < t_T(i); \text{Sol.}(22)) \right] \\ &\quad \left. + H(t_T^{(n)}(i) - t_T(i)) G(t|t_i \leq t < t_T(i); \text{Sol.}(23)) \right] + H(t_i - t_T^{(n)}(i)) G(t|t_i \leq t < t_T(i); \text{Sol.}(24)). \end{aligned}$$

Last, the FID component reads

$$\begin{aligned} G_{\text{FID}}(t|t_T(i) \leq t < t_{i+1}) &= H(t_T^{(f)}(i) - t_T(i)) \left[ H(t_{i+1} - t_T^{(f)}(i)) \right. \\ &\quad \times \left[ H(t_T^{(f)}(i) - t) G(t|t_T(i) \leq t < t_T^{(f)}(i); \text{Sol.}(31)) + H(t - t_T^{(f)}(i)) G(t|t_T^{(f)}(i) \leq t < t_{i+1}; \text{Sol.}(31)) \right] \\ &\quad \left. + H(t_T^{(f)}(i) - t_{i+1}) G(t|t_T(i) \leq t < t_{i+1}; \text{Sol.}(32)) \right] + H(t_T(i) - t_T^{(f)}(i)) G(t|t_T(i) \leq t < t_{i+1}; \text{Sol.}(33)). \end{aligned}$$

Further, we obtain the initial values  $G_i$  for all  $i : 3 \leq i \leq m$  by requiring continuity between the solution branches of the  $(i-1)$ th and  $i$ th injection domain. If the  $i$ th injection enters the system while the  $(i-1)$ th injection is still in the NID and  $S_2 = \emptyset$ , the initial values become

$$G_i = G(t = t_i | t_{i-1} \leq t < t_T(i-1); \text{Sol.}(15)) \quad \text{for } t_i < t_T(i-1),$$

whereas for  $S_2 \neq \emptyset$ , they result in

$$G_i = \begin{cases} G(t = t_i | t_{i-1} \leq t < t_T^{(n)}(i-1); \text{Sol.}(22)) & \text{for } t_i < t_T^{(n)}(i-1) < t_T(i-1) \\ G(t = t_i | t_T^{(n)}(i-1) \leq t < t_T(i-1); \text{Sol.}(22)) & \text{for } t_{i-1} < t_T^{(n)}(i-1) \leq t_i < t_T(i-1) \\ G(t = t_i | t_{i-1} \leq t < t_T(i-1); \text{Sol.}(23)) & \text{for } t_i < t_T(i-1) \leq t_T^{(n)}(i-1) \\ G(t = t_i | t_{i-1} \leq t < t_T(i-1); \text{Sol.}(24)) & \text{for } t_T^{(n)}(i-1) \leq t_{i-1}. \end{cases}$$

If, however, the  $(i-1)$ th injection is already in the FID, we find

$$G_i = \begin{cases} G(t = t_i | t_T^{(f)}(i-1) \leq t < t_i; \text{Sol.}(31)) & \text{for } t_T(i-1) < t_T^{(f)}(i-1) \leq t_i \\ G(t = t_i | t_T(i-1) \leq t < t_i; \text{Sol.}(32)) & \text{for } t_T(i-1) \leq t_i < t_T^{(f)}(i-1) \\ G(t = t_i | t_T(i-1) \leq t < t_i; \text{Sol.}(33)) & \text{for } t_T^{(f)}(i-1) \leq t_T(i-1). \end{cases}$$

### Appendix E: The $CS$ Function

For  $z \in \mathbb{R}_{\geq 0}$ , the  $CS$  function is defined by [15]

$$\begin{aligned} CS(z) &:= \frac{1}{\pi} \int_0^\pi \sin(\theta) \int_{z/\sin(\theta)}^\infty K_{5/3}(y) dy d\theta \\ &= W_{0,4/3}(z) W_{0,1/3}(z) - W_{1/2,5/6}(z) W_{-1/2,5/6}(z), \end{aligned} \tag{E1}$$

where  $K_a$  is the modified Bessel function and  $W_{a,b}$  denotes the Whittaker function [1]. On account of the degree of complexity of (E1), one usually employs an approximate function that is adapted to its asymptotics

$$CS(z) \simeq \begin{cases} a_0 z^{-2/3} & \text{for } z \ll 1 \\ z^{-1} \exp(-z) & \text{for } z \gg 1, \end{cases}$$

where  $a_0 = 1.15$ . Standard approximations are, therefore, given by

$$CS_1(z) := \frac{a_0 \exp(-z)}{z^{2/3}}, \quad CS_2(z) := \frac{a_0 \exp(-z)}{z}, \quad \text{and} \quad CS_3(z) := \frac{a_0}{z^{2/3} (1 + z^{1/3} \exp(z))}.$$

Figure 2 shows the absolute values of the relative deviations of these approximations with respect to (E1) in percent, that is,

$$\text{Dev}(z) := 100 \left| \frac{CS(z) - CS_n(z)}{CS(z)} \right| \quad \text{for } n \in \{1, 2, 3\}.$$

Since the  $CS$  function is used for the computation of the synchrotron intensity, where the spectrum covers the energy range from radio waves to X-rays, i.e., with a lower energy limit of the order neV and an upper limit of the order keV, and  $z = 2\epsilon/(3\epsilon_0\gamma^2)$  with  $\epsilon_0 \sim 10^{-14}b$ , initial electron energies  $\gamma_i \sim 10^4 b^{-1/3}$ , and normalized magnetic field strength  $b \sim 10^{-3}$  up to  $b \sim 10$ , we have to consider values  $z \ll 1$  up to  $z \gg 1$ . Thus, the only suitable choice is the approximate function  $CS_3(z)$ , which coincides with both asymptotic ends of (E1) and has the smallest overall deviation.

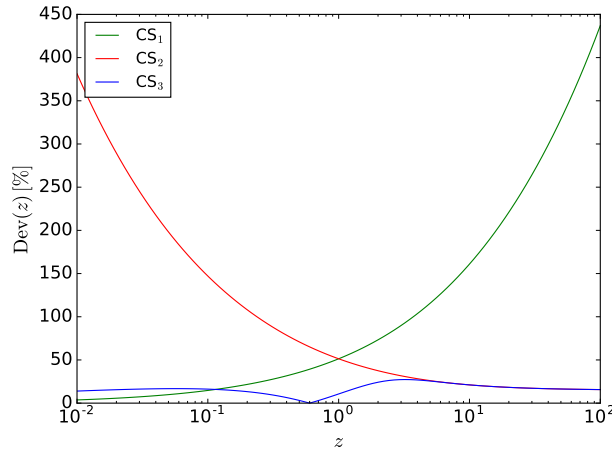


FIG. 2: Absolute values of the relative deviations of the approximate functions  $CS_n$  for all  $n \in \{1, 2, 3\}$  with respect to the exact  $CS$  function in percent.

## Appendix F: Lorentz Transformations

Under the Lorentz transformation from a comoving frame to an observer frame, where quantities in the observer frame are denoted with an asterisk, the energy  $\varepsilon \in \{\epsilon, \epsilon_s\}$  and the time transform according to

$$\varepsilon^* = D \varepsilon \quad \text{and} \quad t^* = \frac{t}{D}$$

with the boost factor

$$D := \frac{1}{\Gamma(1 - \beta \cos(\theta^*))},$$

the angle  $\theta^*$  between the jet axis and the line of sight of the observer, the Lorentz factor  $\Gamma := 1/\sqrt{1 - \beta^2}$ , and  $\beta := v/c$ . For blazars, one can assume that  $\theta^* \searrow 0$  and, thus,

$$D \simeq \sqrt{\frac{1 + \beta}{1 - \beta}}.$$

As the ratio  $I/\varepsilon^3$  is Lorentz-invariant, i.e.,

$$\frac{I(\varepsilon, t)}{\varepsilon^3} = \frac{I^*(\varepsilon^*, t^*)}{(\varepsilon^*)^3},$$

one directly finds that the intensity and the fluence transform as

$$I^*(\varepsilon^*, t^*) = D^3 I(\varepsilon, t) \quad \text{and} \quad F^*(\varepsilon^*) = D^2 F(\varepsilon).$$

## Appendix G: Numerical Code for Fluence SEDs

The numerical implementation of  $G$ , the synchrotron and SSC intensities, as well as the corresponding total fluence SEDs is carried out with Python. Here, we describe the functionality of the code and the specific incorporation of the analytical formulas. The code makes heavy use of the decimal package, which is designed for high floating point precision calculations. This is necessary because the range of possible values between the cooling constants  $D_0$  and  $A_0$ , the injection strengths  $q_i$ , and the inverse injection energies  $x_i$  spans several orders of magnitude, which can lead to a loss of accuracy in expressions where these parameters come up. This problem occurs in its most severe form in the evaluation of the formulas for the transition times  $t_T^{(n)}$  and  $t_T^{(f)}$ , yielding deviations from the expected values by more than 50% with standard floating point precision. But even with higher precision, it is preferable to avoid the evaluation of the transition times altogether. Thus, we compute  $G$  on a grid, using fixed time steps. This makes it possible to read out the values of  $G$  at the grid points and directly compare them to the values of  $G_T^{(n)}$  and  $G_T^{(f)}$  in order to determine the actual solution branch without referring to the transition times.

The code begins with the definitions of the free parameters, namely the injection times  $t_i$ , the injection strengths  $q_i$ , and the inverse injection energies  $x_i$  for  $i : 1 \leq i \leq m$ , the synchrotron and SSC cooling magnitudes  $D_0$  and  $A_0$ , the Lorentz boost  $D$  of the plasmoid, and the upper time boundary of the grid  $t_{\text{end}}$ . The value of  $t_{\text{end}}$  is chosen as one and a half times the injection time of the final injection. In a realistic scenario, however,  $t_{\text{end}}$  corresponds to the end of the observation time. The time grid is set up homogeneously and linearly, and the number of grid points can be chosen arbitrarily. All computations are performed in the plasmoid rest frame. For the later evaluation of the lightcurves and fluences, the relevant quantities are transformed into the observer frame (see Appendix F). Ordered lists of the initial and transition values  $G_i$ ,  $G_T^{(s)}$ ,  $G_T^{(n)}$ ,  $G_T^{(f)}$ , and  $G_T$ , as well as a list keeping track of the elements of the sets  $S_1$  and  $S_2$ , and a list of the various solution branches are implemented. These lists are constantly updated during runtime.

The code constructs  $G$  incrementally in two loops. The first loop covers  $G$  from the time of the first injection  $t = 0$  to the time of the second injection  $t = t_2$  using the solutions (35)-(37). The second loop computes  $G$  from the time of the second injection to the time  $t_{\text{end}}$  employing the solutions (15), (22)-(24), and (31)-(33). During each step, the current time  $t_{\text{cur}}$  is incremented by a fixed value and  $G_{\text{cur}} := G(t_{\text{cur}})$  is determined according to the proper solution branch, which is automatically selected via the above-mentioned lists. Moreover, at each grid point, the analytical expressions for  $G$  are glued together continuously. In more detail, after initializing the values of  $M_1$ ,  $M_2$ ,  $N_1$ ,  $N_2$ ,  $P_1$ , and  $G_T$  at  $t = 0$ , the first loop starts its iteration in the first SID solution branch.



At each step, it evaluates  $G$  at the current time grid point and checks whether  $G_{\text{cur.}}$  exceeds or equals  $G_T^{(s)}$ , i.e., whether  $G$  needs to be expressed by the second SID solution branch. If necessary,  $G$  is altered accordingly and glued to the previous solution branch continuously. Also, if  $G_{\text{cur.}}$  becomes larger than or equal to  $G_T(1)$ , the list for  $S_1$  and  $S_2$  is updated. The loop ends if either  $t_{\text{cur.}}$  exceeds or equals the injection time of the second injection  $t_2$ , or – in a scenario with only a single injection –  $t_{\text{cur.}}$  exceeds the upper time boundary  $t_{\text{end}}$ . In the latter case, the numerical construction of  $G$  is completed. The second loop constructs  $G$  in a similar way as the first loop, but now more cases, which arise from the more elaborate structure of the analytical multiple injection solution, have to be taken into account. Once the second loop ends, the values of  $G$  are known at every point of the grid. This allows us to evaluate the synchrotron and SSC intensities at each grid point by simply substituting these values into the corresponding analytical formulas (42) and (46). The associated total fluences are approximated by sums of the areas of rectangles, each of which is defined by the intensity at the left grid point and the size of the time step. Alternatively, one could implement the approximate analytical formulas derived in Section IV. The total synchrotron and SSC fluence SEDs are then computed as the product of the respective energy and fluence. Since the numbers of grid points and injections can be increased arbitrarily, the precision of these computations is limited only by the machine accuracy and the available CPU time.

- 
- [1] Abramowitz M., Stegun I. A., “Handbook of mathematical functions with formulas, graphs, and mathematical tables,” National Bureau of Standards (1972).
  - [2] Aharonian F. A. et al., “An exceptional very high energy gamma-ray flare of PKS 2155-304,” *The Astrophysical Journal* **664**, L71 (2007).
  - [3] Aharonian F. A. et al., “Simultaneous multiwavelength observations of the second exceptional  $\gamma$ -ray flare of PKS 2155-304 in July 2006,” *Astronomy & Astrophysics* **502**, 749 (2009).
  - [4] Albert J. et al., “Variable very high energy gamma-ray emission from Markarian 501,” *The Astrophysical Journal* **669**, 862 (2007).
  - [5] Biteau J., Giebels B., “The minijets-in-a-jet statistical model and the rms-flux correlation,” *Astronomy & Astrophysics* **548**, A123 (2012).
  - [6] Blandford R. D., Payne D. G., “Hydromagnetic flows from accretion discs and the production of radio jets,” *Monthly Notices of the Royal Astronomical Society* **199**, 883 (1982).
  - [7] Blandford R. D., Znajek R. L., “Electromagnetic extraction of energy from Kerr black holes,” *Monthly Notices of the Royal Astronomical Society* **179**, 433 (1977).
  - [8] Blazejowski M., Sikora M., Moderski R., Madejski G. M., “Comptonization of infrared radiation from hot dust by relativistic jets in quasars,” *The Astrophysical Journal* **545**, 107 (2000).
  - [9] Blumenthal G. R., Gould R. J., “Bremsstrahlung, synchrotron radiation and Compton scattering of high-energy electrons traversing dilute gases,” *Reviews of Modern Physics* **42**, 237 (1970).
  - [10] Böttcher M., “Modeling the emission processes in blazars,” *Astrophysics and Space Science* **309**, 95 (2007).
  - [11] Böttcher M., “Models for the spectral energy distributions and variability of blazars,” arXiv:1006.5048 [astro-ph.HE] (2010).
  - [12] Böttcher M., Reimer A., Sweeney K., Prakash A., “Leptonic and hadronic modeling of Fermi-detected blazars,” *The Astrophysical Journal* **768**, 54 (2013).
  - [13] Cerruti M., Zech A., Boisson C., Inoue S., “Lepto-hadronic modelling of blazar emission,” *Proceedings of the Annual meeting of the French Society of Astronomy and Astrophysics*, 555 (2011).
  - [14] Cerruti M., Zech A., Boisson C., Inoue S., “A hadronic origin for ultra-high-frequency-peaked BL Lac objects,” *Monthly Notices of the Royal Astronomical Society* **448**, 910 (2015).
  - [15] Crusius A., Schlickeiser R., “Synchrotron radiation in a thermal plasma with large-scale random magnetic fields,” *Astronomy & Astrophysics* **196**, 327 (1988).
  - [16] Cui W., “X-ray flaring activity of Markarian 421,” *The Astrophysical Journal* **605**, 662 (2004).
  - [17] Dermer, C. D., Schlickeiser, R., “Model for the high-energy emission from blazars,” *The Astrophysical Journal* **416**, 458 (1993).
  - [18] Eichmann B., Schlickeiser R., Rhode W., “On the duration of blazar synchrotron flares,” *The Astrophysical Journal* **744**, 153 (2012).
  - [19] Felten J. E., Morrison P., “Omnidirectional inverse Compton and synchrotron radiation from cosmic distributions of fast electrons and thermal photons,” *The Astrophysical Journal* **146**, 686 (1966).
  - [20] Ghisellini G., Tavecchio F., Bodo G., Celotti A., “TeV variability in blazars: how fast can it be?,” *Monthly Notices of the Royal Astronomical Society* **393**, L16 (2009).
  - [21] Giannios D., Uzdensky D. A., Begelman M. C., “Fast TeV variability in blazars: jets in a jet,” *Monthly Notices of the Royal Astronomical Society* **395**, L29 (2009).
  - [22] Graff P. B., Georganopoulos M., Perlman E. S., Kazanas D., “A multizone model for simulating the high-energy variability of TeV blazars,” *The Astrophysical Journal* **689**, 68 (2008).
  - [23] Jones F. C., “Calculated spectrum of inverse-Compton-scattered photons,” *Physical Review* **167**, 1159 (1968).

- [24] Kardashev N. S., “Nonstationariness of spectra of young sources of nonthermal radio emission,” *Soviet Astronomy* **6**, 317 (1962).
- [25] Li H., Kusunose M., “Temporal and spectral variabilities of high-energy emission from blazars using synchrotron self-Compton models,” *The Astrophysical Journal* **536**, 729 (2000).
- [26] Marscher A. P., “Turbulent, extreme multi-zone model for simulating flux and polarization variability in blazars,” *The Astrophysical Journal* **780**, 87 (2014).
- [27] Pohl M., Schlickeiser R., “On the conversion of blast wave energy into radiation in active galactic nuclei and gamma-ray bursts,” *Astronomy & Astrophysics* **354**, 395 (2000).
- [28] Reynolds S. P., “Theoretical studies of compact radio sources. II. Inverse-Compton radiation from anisotropic photon and electron distributions: General results and spectra from relativistic flows,” *The Astrophysical Journal* **256**, 38 (1982).
- [29] Röken C., Schlickeiser R., “Synchrotron self-Compton flaring of TeV blazars II. Linear and nonlinear electron cooling,” *Astronomy & Astrophysics* **503**, 309 (2009).
- [30] Röken C., Schlickeiser R., “Linear and nonlinear radiative cooling of multiple instantaneously injected monoenergetic relativistic particle populations in flaring blazars,” *The Astrophysical Journal* **700**, 1 (2009).
- [31] Schlickeiser R., Röken C., “Synchrotron self-Compton flaring of TeV blazars I. Linear electron cooling,” *Astronomy & Astrophysics* **477**, 701 (2008).
- [32] Schlickeiser R., “Non-linear synchrotron self-Compton cooling of relativistic electrons,” *Monthly Notices of the Royal Astronomical Society* **398**, 1483 (2009).
- [33] Schlickeiser R., Lerche I., “Nonlinear radiative cooling of relativistic particles under equipartition conditions I. Instantaneous monoenergetic injection,” *Astronomy & Astrophysics* **476**, 1 (2007).
- [34] Schlickeiser R., Böttcher M., Menzler U., “Combined synchrotron and nonlinear synchrotron-self-Compton cooling of relativistic electrons,” *Astronomy & Astrophysics* **519**, A9 (2010).
- [35] Sikora M., Begerlman M. C., Rees M. J., “Comptonization of diffuse ambient radiation by a relativistic jet: The source of gamma rays from blazars?,” *The Astrophysical Journal* **421**, 153 (1994).
- [36] Sokolov A., Marscher A. P., McHardy I. M., “Synchrotron self-Compton model for rapid nonthermal flares in blazars with frequency-dependent time lags,” *The Astrophysical Journal* **613**, 725 (2004).
- [37] Urry, C. M., Padovani, P., “Unified schemes for radio-loud active galactic nuclei,” *Publications of the Astronomical Society of the Pacific* **107**, 803 (1995).
- [38] Weidinger M., Spanier F., “A self-consistent and time-dependent hybrid blazar emission model,” *Astronomy & Astrophysics* **573**, A7 (2015).
- [39] Yan D., Zhang L., “Understanding the TeV emission from a distant blazar PKS 1424 + 240 in a lepto-hadronic jet model,” *Monthly Notices of the Royal Astronomical Society* **447**, 2810 (2015).
- [40] Zacharias M., Schlickeiser R., “Synchrotron lightcurves of blazars in a time-dependent synchrotron-self Compton cooling scenario,” *The Astrophysical Journal* **777**, 109 (2013).